Journal of the Palaeontological Society of India
Volume 65(1), June 30, 2020: 36-54

ISSN 0552-9360

CLIMATE VARIABILITY IN THE CENTRAL HIMALAYA DURING THE LAST ~15 KYR: EVIDENCE OF PRECIPITATION VARIABILITY FROM MULTIPROXY STUDIES

S. NAWAZ ALI[1*], SHAILESH AGRAWAL[1], M. FIROZE QUAMAR[1], JYOTSNA DUBEY[1], NAVEEN CHAUHAN[2], PINKY BISHT[3], PRATIMA PANDEY[4], MD. ARIF[1], MAYANK SHEKHAR[1] and P. MORTHEKAI[1]

[1]BIRBAL SAHNI INSTITUTE OF PALAEOSCIENCES, LUCKNOW-226007, INDIA
[2]PHYSICAL RESEARCH LABORATORY, AHMEDABAD-38009, INDIA
[3]WADIA INSTITUTE OF HIMALAYAN GEOLOGY, DEHRADUN-248001, INDIA
[4]INDIAN INSTITUTE OF REMOTE SENSING, DEHRADUN-248001, INDIA
[*]Corresponding author e-mail: snawazali@gmail.com

ABSTRACT

The present investigation focuses on understanding and quantifying the climate/precipitation variability for a monsoon–dominated agrarian Indian socio–economy. Samples from a ~3.5 m deep/thick proglacial sedimentary profile, situated on the northern boundary of Indian summer monsoon (ISM) influence, have been used in this study. Important climatic proxies like stable carbon isotope ($\delta^{13}C_{org}$), total organic carbon (TOC), magnetic susceptibility (χ_{lf}), loss on ignition (LOI), and pollen analysis were used for palaeo–reconstructions. The reconstructions are supplemented with optically stimulated luminescence (OSL) ages and provide important insights on the climate variability in the central Himalaya during the last ~15.3 kyr. Based on the results, three phases of negative as well as positive excursions of the precipitation have been identified. A prominent negative precipitation excursion has been observed at ~15 kyr B.P. During ~14–12 kyr B.P., the moisture availability is recorded in moderate values. The later part of this period coincides with the Younger Dryas (YD) cooling event. Moderate moisture availability during YD is attributed to enhanced mid–latitude westerlies that contribute 30-35% of precipitation in this area. Post YD enhancement in precipitation has been observed during ~10.5–8.5 kyr B.P. However, an overall weakening of precipitation during ~8.5–2 kyr B.P. and an increasing trend after 2 kyr B.P. has been observed. The study provides evidence of the strengthening of ISM as well as the mid–latitude westerlies at different time scales during the last ~15.3 kyr and suggests significant moisture contribution from strengthened mid–latitude westerlies during the YD.

Keywords: Stable carbon isotope, palynology, precipitation reconstruction, mid–latitude westerlies, India.

INTRODUCTION

The Indian summer monsoon (ISM) has a major influence on socio–economy of densely populated Indian subcontinent as it brings large amount of summer precipitation to the region that accounts for ~70-80% of the total annual rainfall (Webster *et al*., 1998; Gadgil, 2006). The ISM not only significantly influences the agrarian based Indian economy but is considered as the most significant weather system nourishing the Himalayan glaciers (Finkel *et al*., 2003; Bookhagen and Burbank, 2006; Bookhagen and Strecker, 2008; Yang *et al*., 2008; Meyer *et al*., 2009; Ali and Juyal, 2013). Proxy data from geographically diverse regions of the Indian subcontinent have been used to understand the climate variability during the late Quaternary (Chauhan, 2000; Prassad and Enzel, 2006; Juyal *et al.,* 2009; Bhattacharayya *et al.,* 2011; Leipe *et al.,* 2014; Agrawal *et al.,* 2015; Basu *et al.,* 2015; Ali *et al.,* 2018; Bhushan *et al.,* 2018; Srivastava *et al.,* 2018; Ali *et al.,* 2020a). However, regional high resolution palaeoclimatic records are limited; nevertheless suggest abrupt climate variability that has been catastrophic and associated with the rise and fall of the ancient human civilisations (Witzel, 1987, 1999; Dixit *et al*., 2014; Prasad *et al*., 2014; Sarkar *et al*., 2016). Given the sparse data and complex nature of ISM, its forcing factors are not well understood. The problem gets further enhanced in the Himalayan region, due to limited climate reconstruction records with poorly constrained chronologies. These palaeoclimatic records also have local and regional incongruity and hence the paleoenvironmental and paleoclimatic trajectory in the Himalayan region partly understood (Juyal *et al.,* 2009; Agrawal *et al.,* 2015; Basu *et al.,* 2015; Ali *et al.,* 2018; Bhushan *et al.,* 2018; Srivastava *et al.,* 2018; Banerji *et al*., 2020). Hence, to improve our understanding about the past ISM variability and enhance our predictive capabilities for its future variability, quantitative reconstructions before the instrumental period are required.

Towards this, a multiproxy approach has been used, as different climate proxies have different strengths, weaknesses and sensitivity to different forcing factors (Smol, 2002; National Research Council, 2005; Birks and Birks, 2006). We have used the stable carbon isotope ratios ($\delta^{13}C$) of organic matter associated with sediment/soil (SOM) as a proxy for past climate changes via palaeo-vegetation (Cerling, 1992; Ekart *et al.,* 1999), loss on ignition (LOI) parameters via. moisture, organic and inorganic contents for organic content and productivity. The magnetic susceptibility (χlf) has been used as a proxy for sediment flux (palaeo-environmental conditions), and pollen analysis for palaeo-ecological status and changes in ecosystem/ climate. For palaeo-ISM rainfall reconstruction, $\delta^{13}C_{org}$ ratio and transfer functions proposed by Kohn (2010) and Basu *et al.* (2015, 2019) and successfully used by Ali *et al.* (2018) have been applied. The $\delta^{13}C$ composition of C_3 vegetation has not only been used to reconstruct past climatic conditions but also can be used to estimate the palaeo-precipitation, because carbon isotope ratio of terrestrial C_3 plants and SOM shows a negative correlation with the rainfall amount (Stewart *et al*., 1995; Wang *et al*., 2003; Zheng and Shangguan, 2007; Diefendorf *et al*., 2010; Kohn, 2010; Basu *et al*., 2015; Rao *et al*., 2017). C_3 dominated vegetation zones (alpine vegetation) are located at higher altitude

glaciated regions of the Himalayas (Dubey *et al*., 2018) and the location of present study qualifies this criteria. Besides this, the climatologically sensitive regions (transitional areas) lying between the dry Trans Himalaya/Tibet towards the north and the sub–humid Himalaya towards south have been suggested as important sites for quantitative climatic reconstructions and to understand the ISM variability, as the climate signal here gets amplified and the geomorphic processes respond sensitively to minor changes in precipitation and temperature (Fu, 1992; Srivastava *et al.,* 2013; Wang *et al.,* 2017; Rana *et al.,* 2019; Ali *et al*., 2018, 2020a). The higher Himalaya (glaciated region) has a potential for the reconstruction of the ISM variability during the late Quaternary, as glaciers are considered to be the most sensitive terrestrial recorders of climate change (Ali and Juyal, 2013) and these changes are well preserved in the proglacial sedimentary archives (Ali *et al.,* 2020a). Besides this, there are close interactions among lake level changes with climatic change and the glaciers shrinkage and are preserved in these proglacial sedimentary archives. Therefore, we have focused on the high altitude, pristine proglacial sediment sequence in the Dhauliganga basin of central Himalaya. Our aim is to reconstruct the changes in late Pleistocene–Holocene vegetation associated to ISM variability using palynology, carbon isotope signature ($\delta^{13}C_{org}$) preserved in SOM combined with Loss on ignition (LOI), sediment texture and magnetic susceptibility data. In order to make conclusive correlations with the earlier palaeoclimatic studies from the central Himalaya, we have attempted to synthesize the earlier published palaeoclimatic records. This has been achieved by giving a particular weightage to the climatic classes/inferences drawn in different studies to build an intensity based palaeoclimatic scenario (Herzuch, 2006; Ali *et al.,* 2019).

GEOLOGY AND GEOMORPHOLOGY OF STUDY AREA

We have collected samples from a sedimentary sequence situated in climatologically sensitive Kalla glacier valley (Kuntibanar), Dhauliganga Basin, central Himalaya, Uttarakhand, a transitional zone lying between the dry Trans Himalaya/Tibet towards the north and the ISM dominated sub–humid Himalaya towards the south. The location of this area is important because any relative change (intensification/reduction) in the ISM precipitation will get an amplified signal. Samples for multiproxy studies were collected from a proglacial sedimentary profile (30° 37' 48.18" N and 79° 52' 42.40" E) located on the left side of the Kalla glacier valley at an altitude of ~4000 m asl (Fig. 1). The sampling site is above the tree line and experiences alpine vegetation (Fig. 2). The area lies in the Higher Himalayan Crystalline and is constituted of mica schist, granite, quartzite biotite schist, kyanite schist and augen gneiss of Vaikrita group (Sinha, 1989). Structurally, the study area is bounded by the South Tibetan Detachment System (STDS) in the North and by Main Central Thrust (MCT) in the south (Fig. 1). The STDS defines the tectonic boundary between the higher Himalayan crystalline in the south and Tethyan sedimentary succession in the north (Sinha, 1989; Valdiya, 2001; Juyal *et al.,* 2009; Rana *et al*., 2013; Srivastava *et al.,* 2013; Bisht *et al*., 2015).

Climatologically, Kalla glacier valley is located on the fringe of the ISM dominated central Himalaya. Based on ERA–interim (1958–2001) the temperature data show that July is the hottest month with mean temperature ~17 ˚C, and January the coldest with mean temperature ~ –0.2 ˚C. Moreover, the Tropical Rainfall Measuring Mission data (TRMM) spanning 1998 to 2011 shows that the Mean annual precipitation is ~1194 mm which occurs in monsoon season spread over JJAS and winter precipitation contributes only ~97 mm (DJF), wettest month is July with ~315 mm of precipitation and driest month is November with only ~7 mm precipitation.

MATERIALS AND METHODS

Samples for multiproxy studies were collected from a ~3.6 m deep (thick) sedimentary (proglacial/morainal lake) profile that lies in the proglacial area of the Kalla glacier valley (Figs. 1, 3). A morainal lake is formed by glacial ice and melt-water and is defined as a lake occupying a depression resulting from deposition in an end moraine or ground moraine or between two lateral moraines of a glacier and have a restricted drainage (Bates and Jakson, 1984). The sedimentary profile under investigation is located on the left flank of the Kalla glacier valley, around 2 km upstream of the Garpek village. Field observations and geomorphology suggest that this small lake has a small catchment and was fed by the runoff (glacial/snow melt and rain water) from the northern slopes of the left mountain range (Fig. 3). Lithologically, the profile is dominated by silty sediments and punctuated by sand dominated gritty layers with occasional pebbles (Figs. 3, 4). A total of 72 samples (each representing 5 cm of the sediment profile; ~200 gm) were collected for multiproxy studies.

Optical chronology

Samples for optically stimulated luminescence (OSL) dating were collected in specially designed opaque metal pipes fitted with an O-ring in the cap to avoid moisture leakage (Chandel *et al*., 2006). The samples were opened in controlled laboratory conditions under low intensity red light (Morthekai and Ali, 2014). The samples were treated with 1N HCl and 30% H_2O_2 to remove the carbonates and organic matter respectively. The samples were sieved to obtain 90−150µm grain size fraction. The 90−150µm quartz grains were treated with 40% HF for 80 minutes (etching) with constant magnetic stirring to remove the outer alpha skin (~20 µm) and any remaining feldspar and finally treated with 12N HCL for 30 minutes to remove the fluorides. Infrared stimulated luminescence (IRSL) test was done on all the samples to check the purity of the quartz grains in terms of feldspar contamination. Pre-heat and dose recovery test were also performed to optimize the pre-heat and validate the protocol used respectively. Both the preheat plateau and dose recovery tests were performed on the Sun bleached (5 hours) quartz grains (Fig. 5). Luminescence measurements were made using an automated Risø TL–OSL reader (TL/OSL–DA–20; Bøtter–Jensen *et al*., 2010). The samples were stimulated using blue diode (470±20 nm) and detection optics comprises EMI 9835QA photomultiplier tube coupled with a 7.5 mm Hoya U–340 filter (emission 330±35 nm). Beta irradiations were carried out using an on–plate $^{90}Sr/^{90}Y$ beta source with a dose rate of 3.08 Gy/min.

The equivalent doses (D_e) were measured using modified single aliquot regeneration (double SAR; Murray and Wintle, 2000; Banerjee *et al*., 2001) protocol with preheat of 240°C for 10 s and cut heat of 200°C. The OSL signal was measured at a temperature of 125°C for 40 s and prior to every OSL

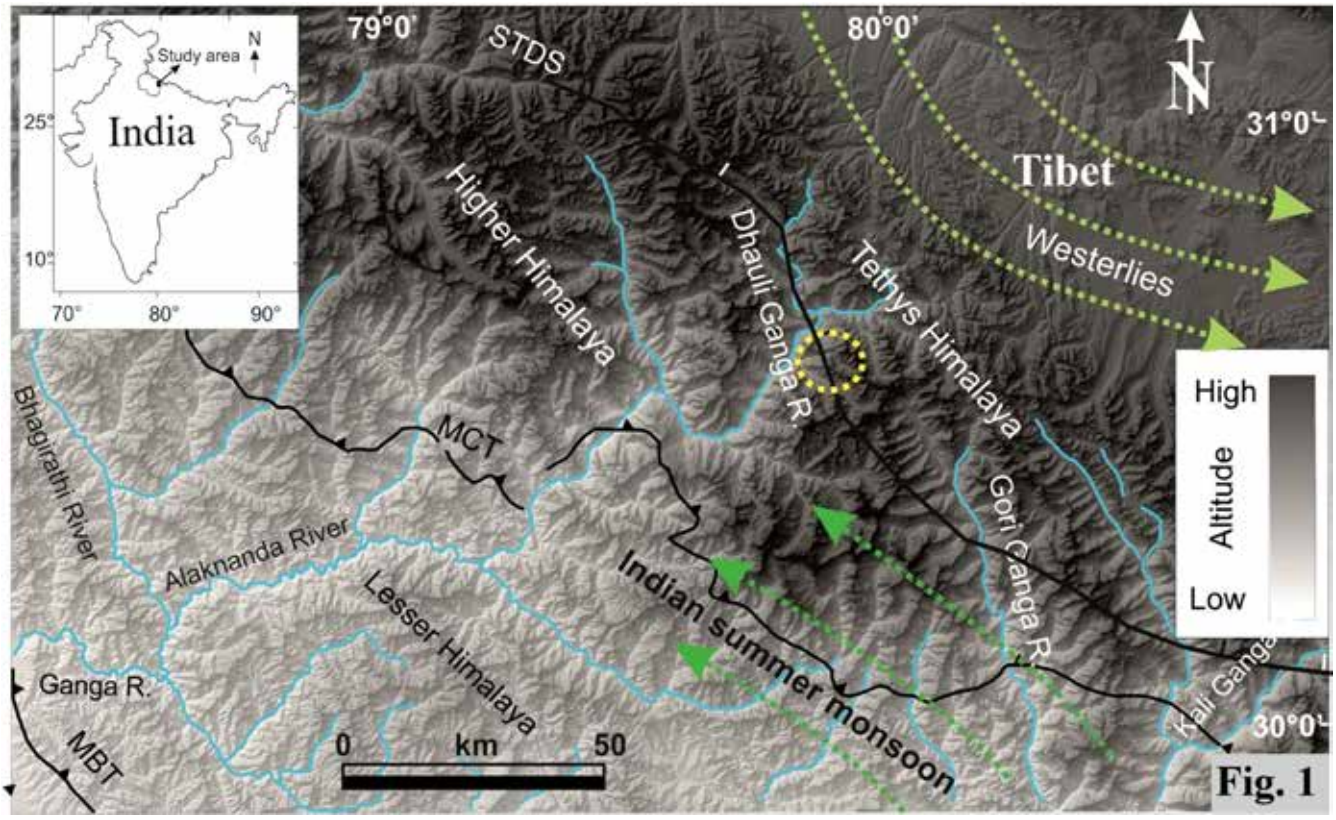

Fig. 1. Shuttle Radar Topographic Mission (SRTM) digital elevation model (DEM) showing the regional setting of the Uttarakhand Himalayas. Study area is shown in dotted yellow circle. The influence of the two major weather systems i.e. the Indian Summer Monsoon (ISM; green dotted arrows) and mid–latitude westerlies (olive green dotted arrows), major drainages as well as major tectonic boundaries are also shown.

measurement, IRSL was measured at 50°C for 100 s to remove any contribution from feldspar. Dose growth curve were constructed using five regeneration dose points including one points to estimate the recuperation and another point to estimate reliability of sensitivity correction (recycling ratio). Finally, for D_e computation we followed central age model (CAM) and minimum age model (MAM3) proposed by Galbraith *et al*. (1999).

The dose rate (annual dose) of the samples was calculated by measuring the concentrations of radioactive material and the conversion factor by Adamiec and Aitken (1998). The concentration of radioactive material i.e. U, Th and K was estimated by using high purity Germanium detector (HPGe) (Table S1). Based on this OSL chronology, ages have been extrapolated to bracket the climatic phases using a Bayesian age depth model and sedimentation rates have been calculated (Parnell, 2016; R-core team, 2017, Fig. 6a). As there is no measured OSL age beyond 280 cm depth, the age depth model yielded a large error. An overall percentage error value of 25% (averaging for the whole profile) was observed (Fig. 6b). Further, the uncertainty for the ages of the strata beyond 280 cm could be larger than estimated because of linear extrapolation irrespective of obvious lithological change.

Table S1. Sample identifier, sample depth, equivalent dose (De), dose rates, over dispersion, radioactivity assays and optical ages obtained from different samples.

Identifier	Depth (cm)	Dose (Gy)	Dose rate (Gy)	OD (%)	U (ppm)	Th (ppm)	K (wt%)	Age (ka)
BP-1*	355				27±0.6	3.02±0.29	3.4±0.06	
BP-2*	315				20.9±0.5	5.44±0.33	2.47±0.05	
BP-3	280	62±3	4.2±0.3	19.6	5.59±0.14	2.18±0.23	2.97±0.06	14.8±1.3
BP-4	240	64±5	6.5±0.4	25.5	11.7±0.3	16.28±0.60	3.14±0.06	9.8±1.1
BP-5	165	48±2	6.1±0.4	10.0	11.3±0.2	6.31±0.24	3.56±0.06	7.8±0.6
BP-7	50	35±3	5.0±0.4	32.7	17.4±0.4	6.27±0.39	0.84±0.03	3.3±0.4
BP-8	20	11±0.4	6.8±0.5	14.5	14.1±0.31	7.01±0.33	3.64±0.07	1.6±0.1

Cosmic ray dose rate = 300±100 (µGy/a; Prescott and Hutton, 1994) and Water content = 10±5 %
**Equivalent dose could not be estimated.*

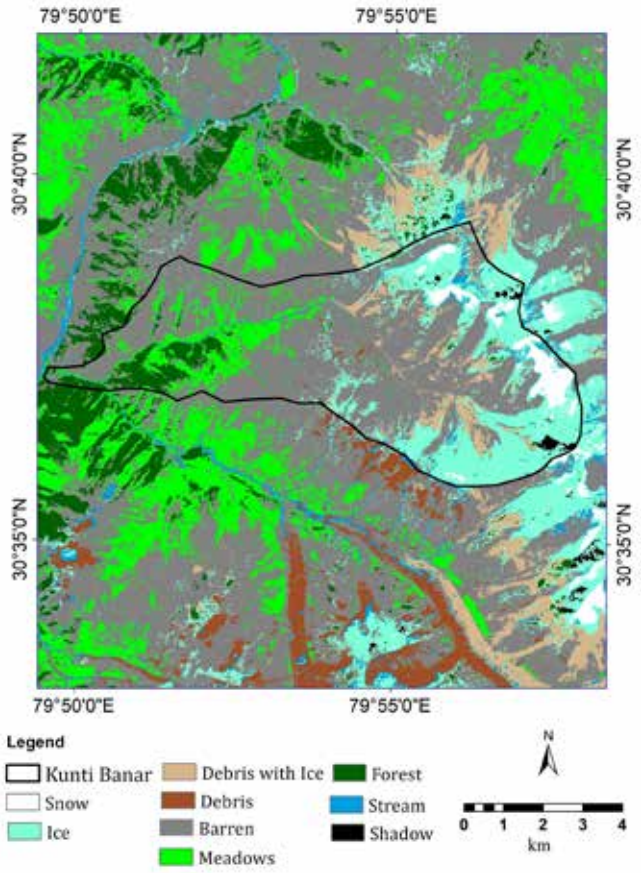

Fig 2. Land–use land cover (LULC) map of the upper reaches of Dhauliganga watershed showing the study area (black line boundary), derived by supervised classification of Landsat 8 imagery. The LULC map has been derived from the satellite data with minimum snow cover and cloud cover.

Total organic carbon (TOC) and carbon isotope ($\delta^{13}C_{org}$) analysis

After coning and quartering, ~1 gm of the sediment sample was taken for isotopic ($\delta^{13}C_{org}$) analysis including TOC. We have followed the sample preparation procedure discussed in Agrawal *et al*. (2015), Dubey *et al*. (2018) and Ali *et al*. (2018). The powdered decarbonated samples were weighed and carefully packed into tin capsules and introduced into the pre–filled and conditioned reactor of Elemental Analyzer (Flash EA 2000 HT). The combusted CO_2 gas was introduced the Continuous Flow Isotope Ratio Mass Spectrometer (CFIRMS, MAT 253) coupled with Con–Flow IV interface for isotopic analysis. IAEA CH3 was used to calibrate the reference gas and carbon isotopic data has been reported against VPDB. International standards (CH3 and CH6) as well as internal standards (Sulfanilamide) were run to check the accuracy for the CO_2 measurements with an external precision of ±0.1‰ (1s). TOC content was calculated from the peak area obtained from sum of the integrated m/z 44, 45 and 46 signals (Jensen, 1991).

Magnetic susceptibility (χ_{lf})

Variation in the magnetic susceptibility indicates changes in the concentration of magnetic minerals and has been used as a proxy for palaeoclimatic reconstruction worldwide (Oldfield *et al*., 1983). In the present study, we have done mass specific magnetic susceptibility (χ_{lf}) measurements of the samples using a Bartington MS2B dual–frequency sensor on a low frequency of 0.465 kHz and x 0.1 sensitivity. Dried samples were homogenized (quartering and coning) and packed in standard 10cc volume plastic vials using a thin foil wrap and weighed. This was followed by making magnetic susceptibility measurements on every sample three times and then the results averaged. Correction for thermally induced drift was done by taking air measurements from time to time between samples measurements.

Palynology

Sample preparation for the extraction of palynomorphs from the sediment samples was carried out following the standard laboratory procedures of maceration technique including acetolysis (Erdtman, 1943; Faegri and Iverson, 1989; Moore *et al*., 1991). We have taken ~10 gm of sediment sample and boiled it in a 10% potassium hydroxide (KOH) aqueous solution for deflocculating the pollen and spores from sediments as well as to dissolve the humus. Following this, these samples were kept in 40% hydrofluoric acid (HF) to remove the silica. Acetolysis (Erdtman, 1943) using a mixture of acetic anhydride and concentrated sulphuric acid in a ratio of 9:1 respectively was done on these samples. The extracts after acetolysis were kept in 50% glycerine solution for microscopic study. On the basis of recovered TPS, the vegetation dynamics and associated climate change was reconstructed. Towards this, the extant surface pollen distribution of the Kalla glacier valley has been used as the reference data for past climate interpretations (Ali *et al.,* 2020b). The pollen spectrum was constructed using TILIA and TILIA Graph in TG View software (Grimm, 1990). Taxa have been grouped according to their life form and ecology (CONISS) and arranged in the pollen spectra as such: trees, shrubs, terrestrial herbs, marshy, algae, aquatics, and fungal spores.

Loss on ignition (LOI)

Total organic content of sediments that is the weight percent of organic matter and carbonate content was estimated by loss on ignition (LOI) technique, based on sequential heating of the samples in a muffle furnace (Bengtson and Enell, 1986; Dean, 1974; Heiri *et al*., 200; Rawat *et al*., 2015; Dubey *et al*., 2018). Five grams of finely powdered sample was taken in a quartz crucible that was kept in an oven at a temperature of 110 °C for 12 hours. Thereafter, the samples were weighed to estimate the percentage of moisture that has been lost from the samples at 110 °C temperature (Eqn. 1). Organic matter was combusted in next step to ash and carbon dioxide at a temperature of 550 °C (2 hours) and weighed further. During the last step, carbon dioxide was evolved from carbonate at 950 °C (2 hours) followed by weighing (Eqn. 1).

$$\text{Loss on ignition (weight \%)} = 100 \times [(n_2 - n_3) / (n_2 - n_1)] \quad (1)$$

Where, n_1 = weight of empty crucible; $n_2 = n_1$ + sample weight (before heating step) and $n_3 = n_1$ + sample weight (after heating step).

Calculation of palaeoclimate index

Following the earlier studies (Herzuch, 2006; Ali *et al.,* 2019), the palaeoclimate indices (pCI) over the central Himalayan region were assigned to indicate the palaeo–monsoon dynamics over the past 34.5 kyr at the interval of 100 years. Based on the intensity of monsoon – highest rank 16 for the intensified monsoon and the lowest rank 1 for dry – as per

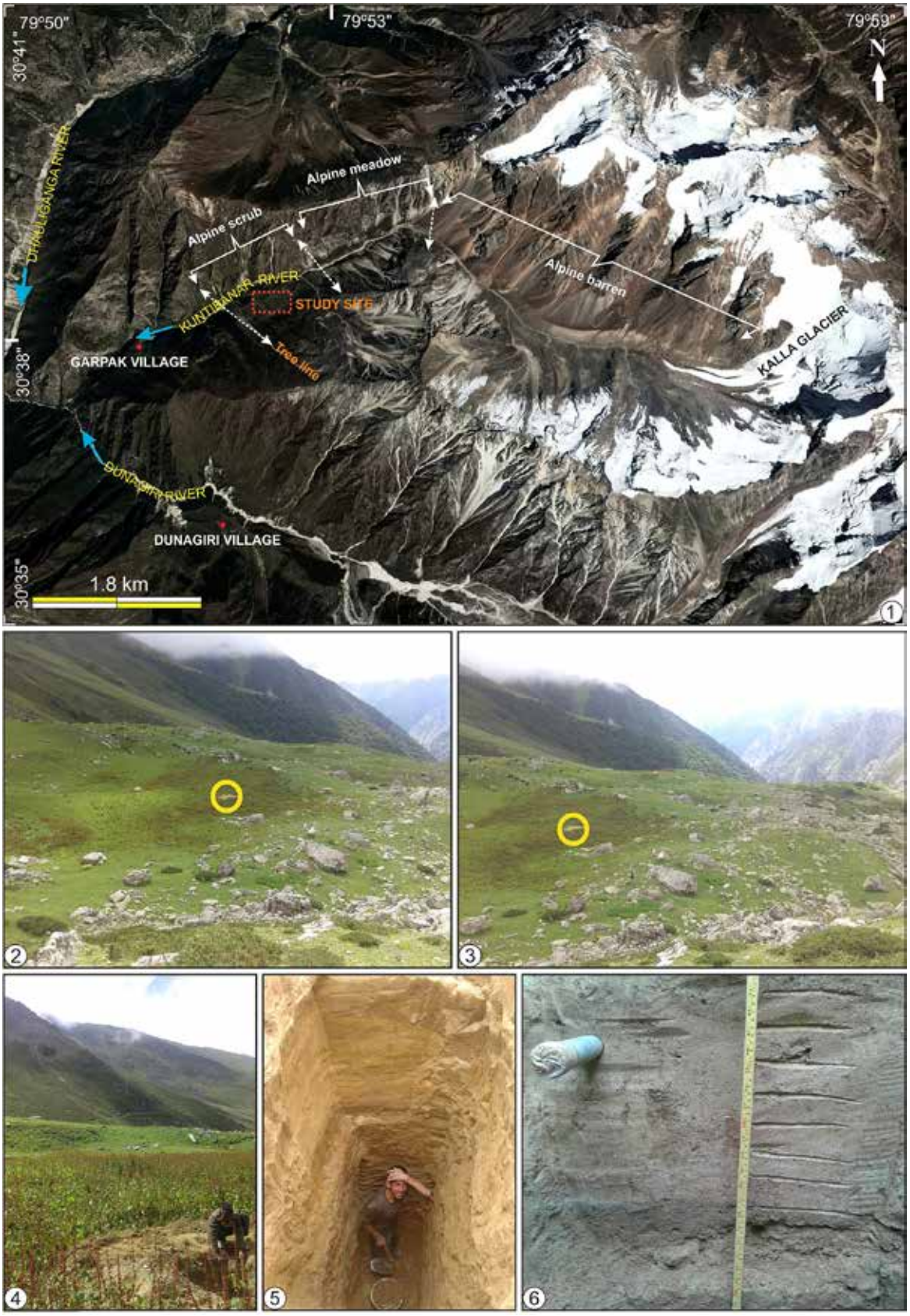

Fig. 3. a) Google Earth Pro imagery of Kalla glacier valley showing the major drainages (blue arrows), settlement (red dots), study area (red dotted rectangle), tree line and three vegetation zones above the tree line i.e. Alpine scrub, Alpine meadow and Alpine barren. b–c) field photographs showing the location of sampling site and a clear demarcation of tree line. d) close up of the sampling site bordered by moraine deposits as seen in the downstream view of the valley. e–f) holistic view of the pit and close up of the sedimentary profile with a metallic pipe used for collecting OSL sample.

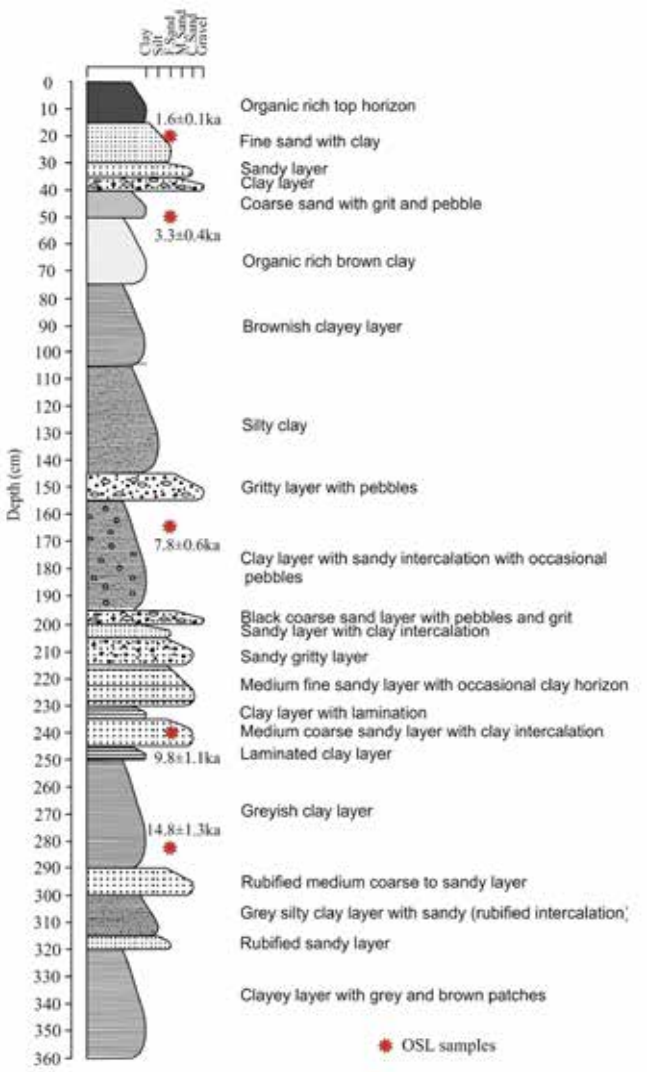

Fig. 4. Litholog of the sedimentary profile showing different stratigraphic units and optically stimulated luminescence ages. Description of the stratigraphic units is given along their sides.

the published literature (27 publications) was assigned (Table S2). The weighted averaging palaeo-climate index (WApCI) was calculated per time slice of 100 a and weight (w_j) was either 1 if the particular time slice has published data or 0 for otherwise (Eqn. 2). The probability density function of WApCI was calculated by normalizing WApCI over the time (Eqn. 3).

$$WApCI = \frac{\sum_j w_j \times pCI_j}{\sum_j w_j}; w_j = \begin{cases} w_j = 1 if\ published\ data\ availabvle \\ w_j = 0 otherwise \end{cases} \quad (2)$$

$$p(WApCI) = \frac{WApCI_t}{\sum_t WApCI_t} \quad (3)$$

where pCI = palaeo–climate index assigned for each time slice of 100 years; (vary from 1 to 16) (Table S2); *w* is the weight, and the subscripts *j* and *t* represent the number of publications and the number of time slices respectively.

TEMPORAL CHANGES IN THE PROXIES

Stable carbon isotope ($\delta^{13}C_{org}$), total organic carbon (TOC) and loss on ignition (LOI) and magnetic susceptibility (χ_{lf})

$\delta^{13}C_{org}$ values for de–carbonated samples in the profile vary from –28.1 to –22.2‰ covering a range of 5.9‰ (mean value –24.9‰). TOC content ranges from ~0.08 to 8.6%. On the basis of the proxies eight (8) climatic zones have been made (Fig. 7; table S3) which are as follows:

Zone–I (355–320 cm; 15.3–14.8 kyr B.P.)

At about 355 cm depth (~15.3 kyr B.P.), the observed $\delta^{13}C_{org}$ value is −26.4‰ which shows gradual enrichment in ^{13}C up to 320 cm depth (14.8 kyr B.P.). This zone has yielded $\delta^{13}C_{org}$ values with an average of −25.1‰ (maximum and minimum values of −23.4 and −26.4‰ respectively). The TOC content is fairly stable and ranges between 0.10 and 0.16%. The LOI shows maximum moisture content of 0.88% and a minimum of 0.4% with an organic content of 2.13 and 0.96%, respectively. The corresponding section has yielded a CO_3% of 3.12 to 2.53. In this zone, the χ_{lf} values are low but show an increasing trend and ranges between 0.39 and 0.67. The maximum χ_{lf} of 0.67 ($^x10^{-8}$ m^3kg^{-1}) occurs at 335 cm depth and minimum χ_{lf} of 0.39 ($^x10^{-8}$ m^3kg^{-1}) occurs at 350 cm depth (Fig. 7). It is to be noted that the age bracket is based on 50 percentile value and the uncertainty in the age estimates are high for this zone (27%; 4 ka). Hence change in the proxy values during 15.3 – 14.8 ka (0.5 ka) need to be validated by age estimates at this zone.

Zone–II (320–290 cm; 14.8–14.2 kyr B.P.)

In this zone, $\delta^{13}C_{org}$ values ranges between −25.6 and −26.6‰ with an average of −26.0‰. This zone has yielded relatively more negative $\delta^{13}C_{org}$ values. While, the TOC content shows a similar trend as zone I, and range between 0.10 and 0.15%. Maximum and minimum moisture content estimated for this zone through LOI is 1.09% and 0.59% with an organic content of 2.28 and 1.50%, respectively. The corresponding section has yielded a CO_3% of 2.8 to 1.17. The χ_{lf} values show a decreasing trend and ranges between 0.17 and 0.58. The maximum χ_{lf} of 0.58 ($^x10^{-8}$ m^3kg^{-1}) occurs at 320 cm depth and minimum χ_{lf} of 0.17 ($^x10^{-8}$ m^3kg^{-1}) occurs at 290 cm depth (Fig. 7). A cautionary note need to be served on the uncertainty of ages (22 %; 3.2 ka) for this zone (duration of 0.6 ka) as well.

Zone III (290–260 cm; 14.2–12.1 kyr B.P.)

This zone is characterized by relatively higher $\delta^{13}C_{org}$ values ranging between −25.3 and −24.7‰ with an average value of −25.1‰. TOC content shows monotonous increasing trend with values of 0.17 to 0.35. In this zone moisture content ranges between 2.12% and 1.31% with an organic content of 2.13 and 0.96%. CO_3% in this zone ranges between 3.23 and 1.15. The χ_{lf} values are much lowered and show an increasing trend that ranges between 0.3 and 0.4. The maximum χ_{lf} of 0.4 ($^x10^{-8}$ m^3 kg^{-1}) occurs at 265 cm depth and minimum χ_{lf} of 0.3 ($^x10^{-8}$ m^3 kg^{-1}) occurs at 285 cm depth (Fig. 7). Unlike Zone I and Zone II, the uncertainty in the ages is 17 % (2.2 ka) and it is comparable with the duration of this zone (2.1 ka). Hence the observed changes in the proxy values are likely be labeled for this time period.

Zone IV (260–195 cm; 12.1–8.8 kyr B.P.)

The $\delta^{13}C_{org}$ values in this zone show an overall decreasing trend with an average value −26.6‰ (max. −25.6‰; min.

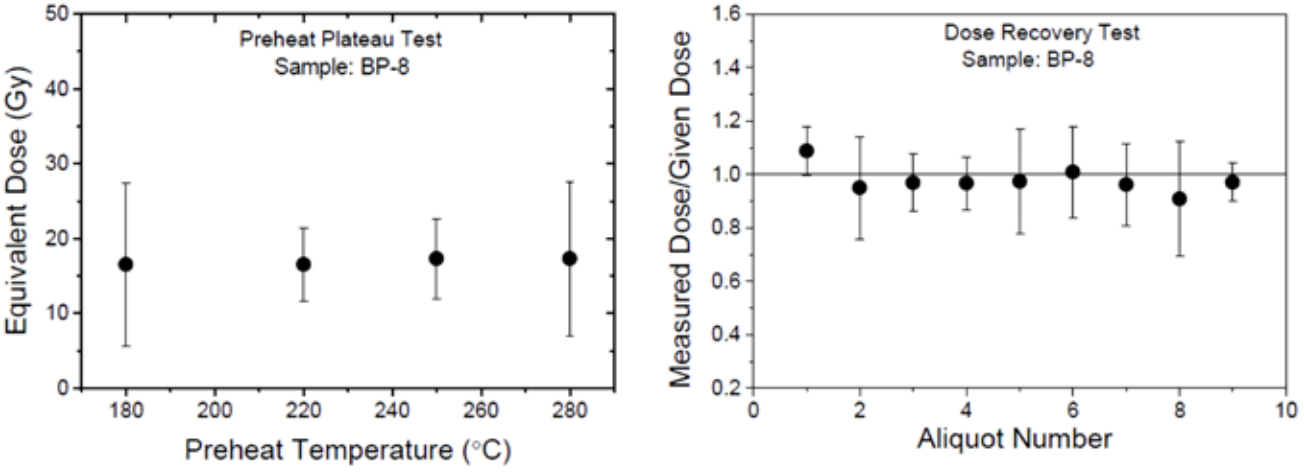

Fig. 5. Preheat plateau and dose recovery test.

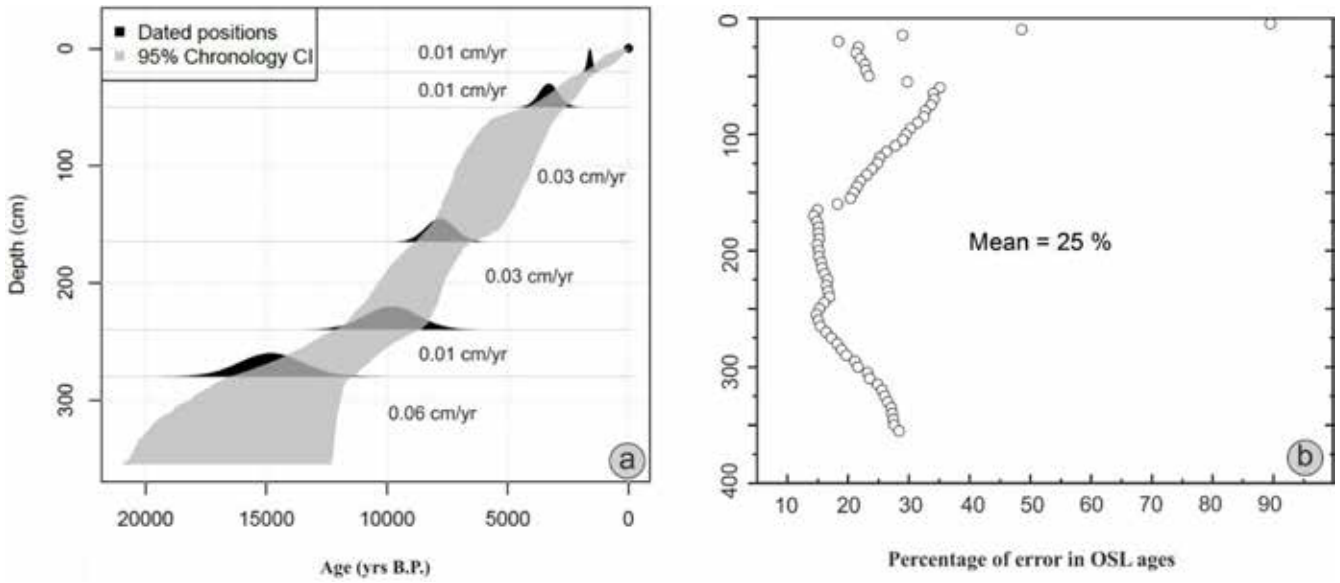

Fig. 6. (a) Bayesian age depth model with sedimentation rate and (b) figure showing the errors along the whole profile.

−27.1‰). This zone shows relatively low TOC content (0.08 to 0.17). A maximum moisture content of 3.96% and a minimum of 0.26% with an organic content of 1.87 to 0.62% is observed. This section has yielded a CO_3% of 4.21 to 1.15. The χ_{lf} values sharply increases at 10.3 kyr B.P. and then it decreases slowly at 10–9.8 kyr B.P. From there, it increases further at 9.7 kyr B.P. and decreases later on. This increasing behavior of χ_{lf} is abnormal as the other values were constant between 0.46 and 0.52. Here the χ_{lf} ranges between 0.28 and 0.72. The maximum χ_{lf} of 0.72 ($^{x}10^{-8}$ m^3kg^{-1}) occurs at 245 cm depth and minimum χ_{lf} of 0.28 ($^{x}10^{-8}$ m^3kg^{-1}) occurs at 195 cm depth. Uncertainty in the ages for this zone is 16 % (1.4 ka) which is well below than the duration of this zone (3.3 ka), and this is the case for the zones to come (Zones V – VIII; Fig. 7).

Zone V (195–120 cm; 8.8–6.0 kyr B.P.)

In this zone, $\delta^{13}C_{org}$ values ranges between −26.7 and −22.2‰ with an average of −24.1‰. This zone shows an overall increasing trend in $\delta^{13}C_{org}$ values and highest values are observed at about ~6.2 kyr B.P. The TOC content in this zone range between 0.10 to 0.28%. Moisture content ranges between 5.93% and 0.72% with an organic content of 3.40 and 1.68%. CO_3% in this zone ranges between 3.88 and 1.89. The χ_{lf} values show both increasing and decreasing trend. The χ_{lf} increases from 8.5–7.4 kyr B.P (Fig. 7). and then follow a decreasing trend till 6 kyr B.P. The χ_{lf} ranges between 0.32 and 0.69. The maximum χ_{lf} of 0.69 ($^{x}10^{-8}$ m^3kg^{-1}) occurs at 160 cm depth and minimum χ_{lf} of 0.32 ($^{x}10^{-8}$ m^3kg^{-1}) occurs at 135 cm depth .

Zone VI (120–75 cm; 6.0–4.3 kyr B.P.)

The $\delta^{13}C_{org}$ values and TOC content range between −22.8 to −23.2‰ and 0.17 to 0.46% respectively. This zone shows maximum moisture content of 1.87% and a minimum of 0.64% with an organic content of 5.19 and 1.76%, respectively. This section has yielded a CO_3% of 2.55 to 1.80. The χ_{lf} values are mostly constant throughout this zone and ranges between 0.31 and 0.49. The maximum χ_{lf} of 0.49 ($^{x}10^{-8}$ m^3kg^{-1}) occurs at 95 cm depth and minimum χ_{lf} of 0.31 ($^{x}10^{-8}$ m^3kg^{-1}) occurs at 115 cm depth.

Zone VII (75–25 cm; 4.3–1.9 kyr B.P.)

The $\delta^{13}C_{org}$ values range from −24.0 to −22.9‰ with an average of −23.5‰. TOC range from 0.10 to 0.60% and shows overall increasing trend up to 3.3 kyr B.P. followed by decreasing trend. The maximum moisture content in this zone is 2.15% and minimum is 0.33% with an organic content of 5.50 and 1.09%, respectively. This section has yielded a CO^3% ranging between 2.63 and 1.12. In this zone, the χ_{lf} show both decreasing and increasing trend. The χ_{lf} decreases from 4.1–3.7 kyr B.P. and then increases sharply at 3.5 kyr B.P. Afterwards, it decreases till 3 and increases at 2.7 kyr B.P. and decreases further on (Fig. 7). The χ_{lf} ranges between 0.28 and 0.79. The maximum χ_{lf} of 0.79 ($^{x}10^{-8}$ m^3kg^{-1}) occurs at 55 cm depth and minimum χ_{lf} of 0.28 ($^{x}10^{-8}$ m^3kg^{-1}) occurs at 45 cm depth.

Zone VIII (25–0 cm; ~1.9 kyr B.P.–present)

In this zone the $\delta^{13}C_{org}$ values range from −28.1 to −25.1‰. TOC range from 0.7 to 8.6% and shows overall increasing trend. The maximum moisture content in this zone ranges between 8.35 and 0.60% with an organic content of 20.28 and 2.88%, respectively. The corresponding section has yielded a CO^3% of 2.12 to 1.36. The χ_{lf} values are constant until 1.2 kyr B.P. and show a sudden increase at 0.8 kyr B.P. and decreases further on. The χ_{lf} ranges between 0.35 and 0.74. The maximum χ_{lf} of 0.74 ($^{x}10^{-8}$ m^3kg^{-1}) occurs at 10 cm depth and minimum χ_{lf} of 0.35 ($^{x}10^{-8}$ m^3kg^{-1}) occurs at 20 cm depth.

Precipitation reconstruction

Basu *et al*. (2015) showed that bulk $\delta^{13}C_{org}$ value of C_3 plant in the Gangetic plain, India increases by 0.4‰ with a decrease in rainfall amount by 100 mm. Two major compilations (Kohn, 2010; Diefendorf *et al*., 2010) of $\delta^{13}C_{org}$ values of C_3 plants and their relationship to change in rainfall amount indicated that the end member threshold values for pure C_3 plants can vary depending on the MAP at a location. Further, Rao *et al*. (2017) showed that the $\delta^{13}C_{org}$ values of modern plants and surface soils under pure C_3 vegetation at globally distributed sites are significantly negatively correlated with MAP. All these studies confirming that the $\delta^{13}C_{org}$ of organic matter sourced from pure C_3 vegetation can be used for quantitative paleoprecipitation reconstruction. In this series, quantitative palaeoprecipitation reconstruction based on $\delta^{13}C_{org}$ values has been applied to study Europian loess (Hatte *et al*., 2001), the loess of the western China Plateau (Rao *et al*., 2013) and glacial outwash sediments from the Sikkim Himalaya (Ali *et al*., 2018). Kohn (2010) compiled and modeled the $\delta^{13}C_{org}$ values of modern C_3 plants and suggested that the $\delta^{13}C_{org}$ values of modern C_3 plants are the factors of altitude, latitude and MAP. Therefore, in the present study with the help of $\delta^{13}C_{org}$ value, latitude and elevation the mean annual rainfall have been calculated for the region using the following equation given by Kohn (2010).

$\delta^{13}C_{org}$ (‰, VPDB) = −10.29 + 1.90 × 10^{-4} Altitude (m) − 5.61log10 (MAP + 300 mm/year) − 0.0124 Abs (latitude°).

(note: The equations developed by Kohn (2010) has a threshold limit and is suggested to be used effectively for the values of $\delta^{13}C < -23$ to > -31.5‰. Therefore, we suggest that the reconstructed precipitation values in the present study should be considered effective only within above mentioned isotopic range).

In the present study, we have used 100 yr average CRU data (Harris *et al*., 2014) of precipitation and cross checked our modern $\delta^{13}C_{org}$ based precipitation values with it. The correlations

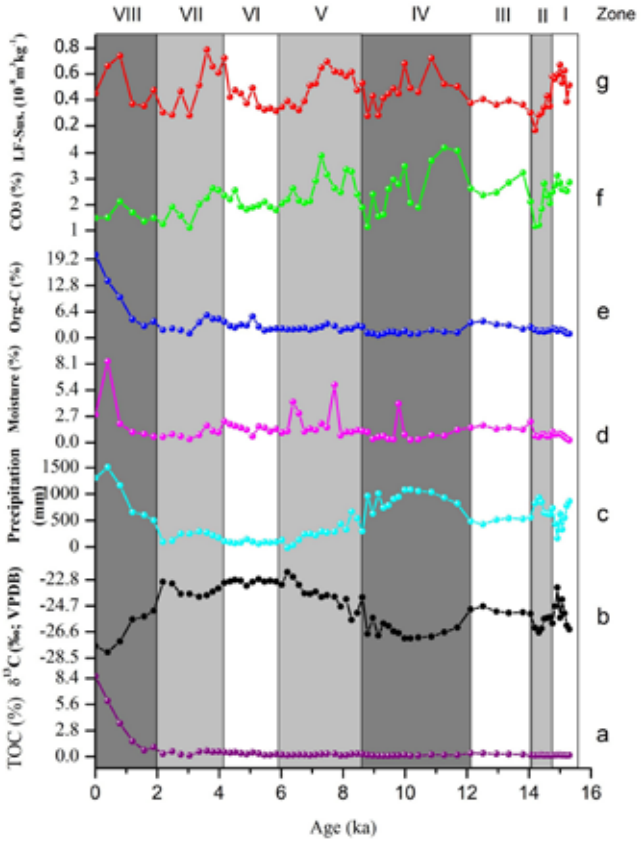

Fig. 7. Line graph of the multiproxy data used in this study. The bottom purple line (a) of the graph represents the TOC (%) values; (b) the black line represents the $\delta^{13}C$ value (‰; VPDB); (c) the turquoise line represents the reconstructed precipitation; (d) the pink line shows the moisture (%) content; (e) organic carbon (%) is represented by blue line; (f) the green line represents the carbonate (%) values and (g) the red line represents low field magnetic susceptibility.

are significant and hence suitable for palaeoprecipitation reconstructions for the last ~15.3 kyr B.P. At the base of the profile (~15.3 kyr B.P.) the $\delta^{13}C_{org}$ based precipitation reconstruction suggest that the study area was receiving an annual precipitation of ~880 mm that show a gradual decline towards the top of Zone I and recording a minimum precipitation of ~250 mm (Fig. 7). Our $\delta^{13}C_{org}$ values based monsoon rainfall reconstruction for Zone II show highest precipitation i.e. ~960 mm during ~13.9–12.3 kyr B.P. Interestingly, during the YD i.e. Zone III an overall decrease in the precipitation is observed and minimum values going as low as ~440 mm. Strengthening of the rainfall post YD cooling event is very clear in Zone IV (~10.5–8.5 kyr B.P.). During this period a maximum precipitation of ~1150 mm is recorded at ~9.8 kyr B.P. During the succeeding period zones (Zone V to VII), the area has recorded the lowest precipitation and has been as low as ~160 mm i.e. out of the empirical relation range (~6.2 kyr B.P.). Gradual strengthening in the annual precipitation is recorded in the topmost zone (Zone VIII) with maximum value reaching to ~1746 mm.

Palynology

On the basis of the varying frequencies of the prominent arboreals and non–arboreal taxa the altitudinal pollen spectra within the area were subdivided into four pollen assemblage zones (BP–I, BP–II, BP–III & BP–IV) to interpret the temporal

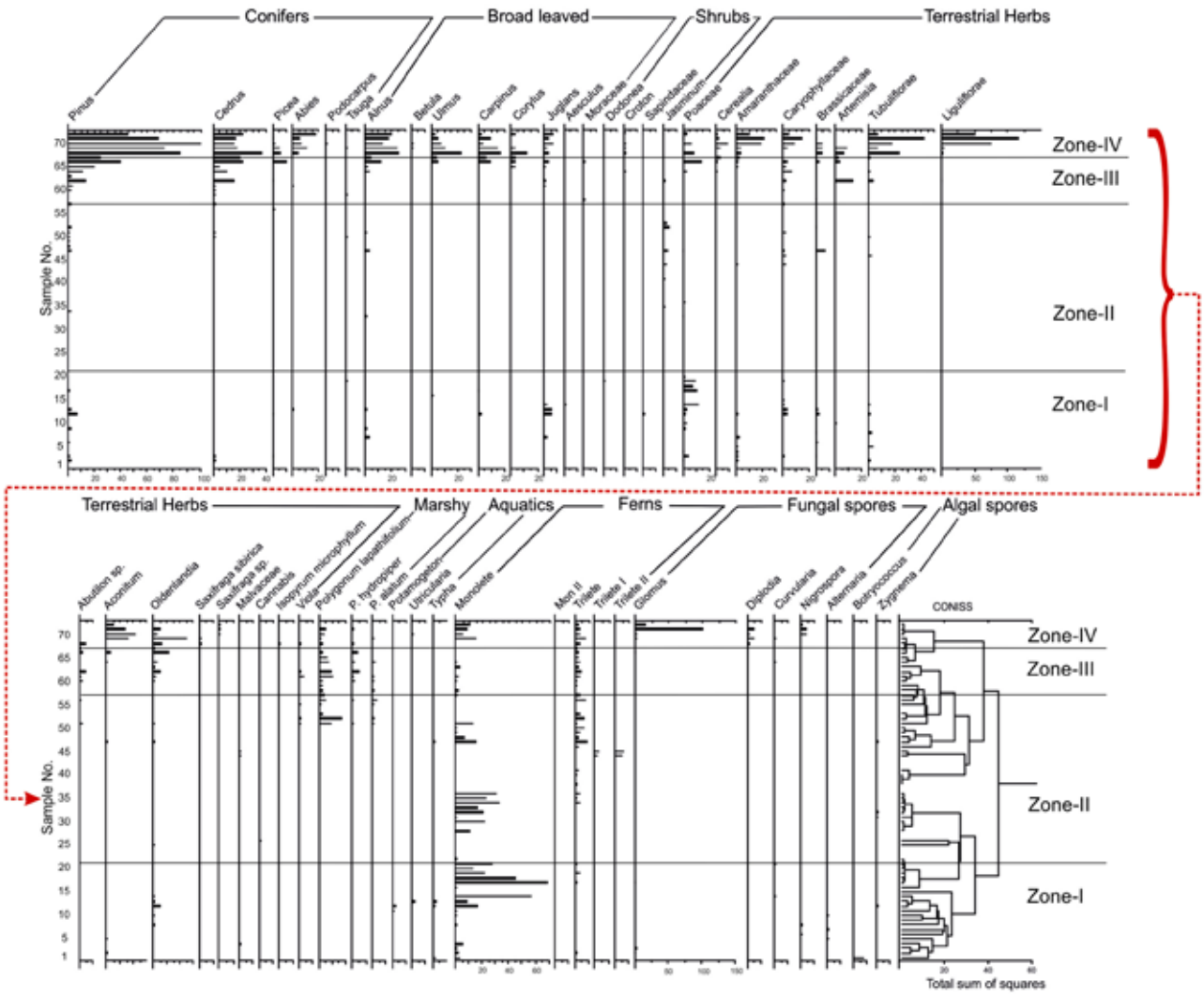

Fig. 8. The Pollen spectra of sedimentary profile showing percentage and concentration of different pollen taxa (table S4).

Table S2. Climatic scenario and their Weightage used for the line diagram. (Increasing trend in the Weightage represents increase in the precipitation/ wetter climate).

Climatic inference	Weightage
Cool and dry climate	1
Dry climate	2
Cool and dry with an ameliorating trend	3
Warm and dry climate (weak ISM)	4
Warm and less humid with (weak ISM)	5
Warm and relatively less humid climate with weak ISM	6
Warm and humid climate	7
Warm and relatively more humid	8
Relatively warm and humid with moderate ISM precipitation	9
Warm and more humid with timely advent of ISM	10
Warm and humid with increased ISM precipitation	11
Warm and more humid with increased ISM precipitation	12
Warm and less moist with weak ISM	13
Warm and moist	14
Warm and more moist with the onset of active ISM	15
Warm and more moist with strong ISM	16

vegetation dynamics and contemporary climate in the region. The zones are designated with the initials 'BP' after the name of the site of investigation, Biskim (Fig. 8). The pollen zones numbering from bottom to top are described as below:

Pollen Zone BP–I (355–250 cm; 15.3–11.3 kyr B.P.)

The pollen assemblage (*Pinus–Cedrus–Picea–Alnus–Carpinus–Juglans–Aesculus*–Poaceae–Amaranthaceae–Caryophyllaceae–Brassicaceae–Tubuliflorae/Asteroideae–Malvaceae–*Aconitum–Oldenlandia*) of this zone is characterized by sporadic representation of arboreal and non–arboreal taxa, thus constituting the open mixed coniferous/ broad–leaved forest under a less cold and dry climate with reduced monsoon precipitation. *Pinus* sp. represents highest pollen frequency and the value ranges from 8.3% to 33.5% followed by other conifer taxa like *Cedrus* sp. (10–12.5%) and *Picea* sp. (2.8–10%) recorded sporadically in the pollen count with high frequency. However, *Abies* sp. and *Tsuga* sp. is represented only in sample BP–13 and BP–19 with frequency of 5% and 7.7% respectively. Among the broad–leaved taxa, *Alnus* sp. represents higher values (5– 43%). However, other broad leaved taxa such as *Ulmus* sp. and *Carpinus* sp. (7.7–8.3%) are recorded sporadically from low

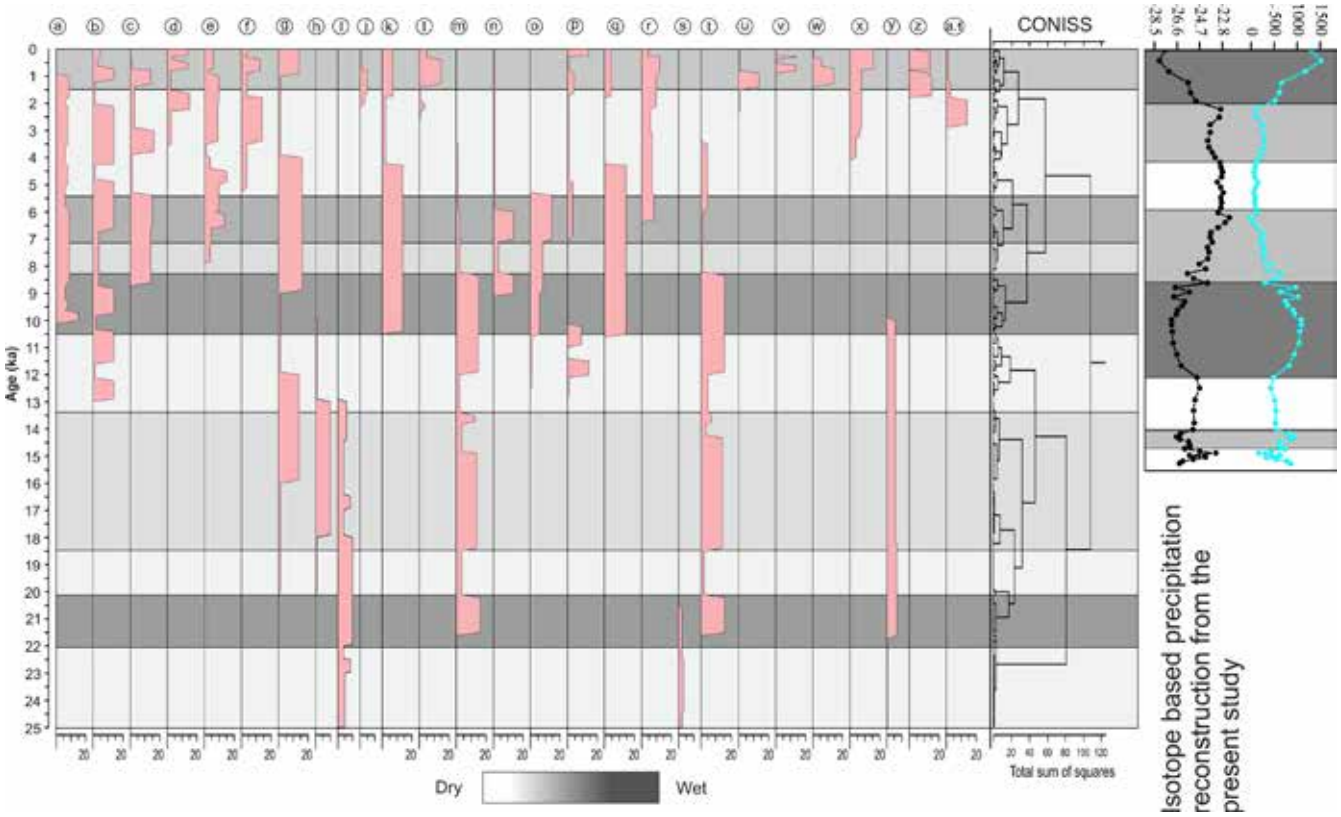

Fig. 9. Synthesis of climate variability using weighted climatic interpretation based on the inferences drawn in different studies from the central Himalayas (data given in table S5 and for Weightage please refer to table S1), India with CONISS Cluster analysis and probability density plot. The ascending order of the scale (0–20) represents intensification of the monsoon. Inferences from the following studies have been used to reconstruct the review plot. **a)** Bhushan *et al*., 2018; **b)** Rawat *et al*., 2015; **c)** Srivastva *et al*., 2018; **d)** Ruhland *et al*., 2006; **e)** Phadtare, 2000; **f)** Kotlia and Joshi, 2013; **g)** Pant *et al*., 2005; **h)** Juyal *et al*., 2004; **i)** Juyal *et al*., 2009; **j)** Kar *et al*., 2002; **k)** Ranhotra and Bhattacharyya, 2010; **l)** Chauhan and Sharma, 2000; **m)** Kotlia *et al*., 2013; **n)** Bhattacharyya *et al*., 2011; **o)** Bhattacharyya *et al*., 2006; **p)** Bali *et al*., 2015; **q)** Chakraborty *et al*., 2006; **r)** Bali *et al*., 2017; **s)** Kotlia *et al*., 2008; **t)** Kotlia *et al*., 2010; **u)** Chauhan *et al*., 2000; **v)** Bhattacharyya and Chauhan, 1997; **w)** Chauhan, 2006; **x)** Kotlia *et al*., 2015; **y)** Kotlia, 2000; **z)** Sanwal *et al*., 2013; **a.1)** Chauhan *et al*., 1997.

to high frequencies. *Juglans* sp. (11.1–28.6% pollen) is noted with high value and *Aesculus* sp. (5.6% pollen) is represented only in one sample (BP–14) in this zone showing a moderate value. Shrubby taxa such as *Dodonea* sp. (7.7%), *Sapindus* sp. (2.8%) and *Croton* sp. are recorded in extremely low values.

Among the non arboreals Poaceae sp. shows the highest frequency with values ranging between 12.5 and 83% in total pollen sum. While other cultural pollen taxa such as Amaranthaceae (3–33%), Caryophyllaceae sp. (5.5–8.5%) and Brassicaceae (10–67%) contribute significantly higher values with sporadic representation in the pollen rain. Tubuliflorae (Asteroideae of the Asteraceae family, 2.9–12.5% pollen) representing higher value is followed by other terrestrial herbs such as *Aconitum* sp. (12.5–16.7%), *Oldenlandia* sp. (5–14%) while, Malvace is represented by a high frequency of 33.3% in sample BP–4. *Potamogeton,* the aquatic taxon, are recorded in moderate value of (5%), whereas *Utricularia* records value of ~10%. Zygospore of *Zygnema,* the algal spores is represented in extremely moderate value of 2.8%. Monolete fern spore records a high frequency (1–69%) while trilete appears inconsistently in low to high frequencies (1.4–15.3%). The fungal spores such as *Glomus* sp., *Curvularia* sp., *Nigrospora* sp., *Typha* sp. and *Alternaria* sp., are recorded in extremely low frequency. Of the algal morphs, considerably high values of *Botryococcus* (58.3%) are noticed in this pollen zone.

Pollen Zone BP–II (250–90 cm; 11.3–4.9 kyr B.P.)

The pollen assemblage *(Pinus–Cedrus–Picea–Jasminum–* Amaranthaceae–Caryophyllaceae–Brassicaceae–Tubuliflorae/ Asteroideae–*Polygonum lapathifolium–Polygonum alatum–* Malvaceae) of this zone indicates savannah– type vegetation occupied the landscape around the study area under a cold and dry with a relatively reduced monsoon precipitation. The pollen in this zone, though, are scantily recorded, making it difficult to draw a clear inference of the vegetation changes and associated with past climate. *Pinus* sp., *Cedrus*, *Picea* , *Abies* are the conifers among arboreals recorded sporadically in variably low to high frequencies. *Jasminum* sp. a shrubby element is scantily recorded in the pollen rain.

Among the conifers/needle-leaved tax, *Pinus* sp. is recorded in high frequency with an average value of 4.1–60%. The pollen of other conifers such as *Cedrus* sp. (10–25% pollen), *Tsuga* sp. (25–50%) and *Picea* sp. (16.7% pollen) are recorded in extremely low frequencies and are sporadically recorded.

Alnus sp., a broad–leaved taxa, is recorded only in one sample with a frequency of 4.2% in this pollen zone. Among the non–arboreal taxa, Poaceae is represented sporadically in the palynoassemblage within a range of 4.16%. However, Amaranthaceae sp. (12.5%) along with other cultural pollen taxa like those from the families Caryophyllaceae sp. (8.3–25%),

Brassicaceae sp. (3.9–35%) were encountered sporadically in moderate to high values in the palynoassemblage.

Tubuliflorae/Asteroideae (25–50%) along with other terrestrial herbs, such as *Abutilon* sp. (8.3%), *Aconitum* sp. (5%) and *Oldenlandia* sp. (4.1%) are represented sporadically in low to moderately high values while Malvaceae is represented comparatively in higher values (12.5–16.7%). However, *Viola* sp. is sporadically represented in the palynoassemblage ranging from 3.8–4%. The marshy taxa such as *Polygonum lapathifolium* (25–65.4%), *Polygonum hydopiper* (4.16–8.3%) and *Polygonum alatum* (3.8–25%), appears inconsistently in variably moderate to high values. Zygospores of *Zygnema,* the algal spores appeared in high values with an average of ~8.5% (100). Monolete and trilete fern spores are recorded with high frequency ranging between 1–96% and 40.1–75% respectively. Also, this zone does not experience the representation of other fungal spores as compared to the preceding pollen zone.

Pollen Zone BP– III (90–25 cm; 4.8—1.9 kyr B.P.)

The pollen assemblage (*Pinus–Cedrus–Picea–Alnus–Carpinus– Ulmus* –Moraceae–Poaceae–Caryophyllaceae – Brassicaceae *–Artemisia–Oldenlandia–Viola– Polygonum lapathifolium–Polygonum hydopiper–Polygonum alatum*) of this zone shows the presence of mixed coniferous/broad-leaved forest in the region. The recovered pollen assemblages have shown much higher frequencies of conifers among the arboreals and low values of non–arboreals. The values of *Pinus* sp. (14.3–47.6% pollen) increased comparatively so as the values of *Cedrus* sp. (7.1–27.4% pollen) in this pollen zone. Other coniferous elements such as *Picea* sp. (1.3–6.4%) records a high frequency in the pollen rain although *Abies* sp. (3.8%) are recorded in moderate frequencies and *Tsuga* sp. has maintained its low record. Among the broad leaved taxa the pollen of *Alnus* sp. (4.7–7.8%), *Ulmus* sp. (3.2–5.5%), *Carpinus* sp. (2.3–8.2%), *Corylus* sp. (1.2–4.3%), *Juglans* sp. (1.3–2.4%) are encountered in moderate to high frequencies but they have increased as compared to the preceding pollen zone. Moraceae appeared for the first time with a very low pollen frequency (0.64–16.7%). However, the pollen frequency of *Jasminum* sp. has reduced to a very low value (1.3%) as compared to other pollen zones.

Poaceae is recorded in very low values (average ~ 2.3–9%) as compared to the preceding pollen zones, whereas Cerealia appears first time in this pollen zone showing very low pollen frequency with an average 0.6–4%. Other cultural pollen taxa such as Amaranthaceae sp. (0.6–2.7%), Caryophyllaceae sp. (1.9–13.5%), Brassicaceae sp. (1.3–17%), *Artemisia* sp. (1.9–17%) are encountered sporadically in high values. Tubuliflorae/ Asteroideae (1.4–1.9%) and Liguliflorae/Cichorioideae (1.3%) were encountered in trace amounts. The other terrestrial herbaceous taxa contributing to the total pollen rain, though in low to high values are *Abutilon* sp. (1.3–14.3%), *Aconitum* sp. (1.9%) and *Oldenlandia* sp. (1.3–7.7%). However, *Viola* sp. is sporadically represented in the pollen rain with value ranging between 1.3 and 11.5%.

Polygonum lapathifolium (1.2–38.5%), *Polygonum hydopiper* sp. (3.8–16.7%) and *Polygonum alatum* (2.6–14.3%) are the marshy taxa recorded in high values showing a considerable increase in pollen frequency in this zone. Monolete and trilete fern spores remained more or less in high frequency as in the preceding zone with a value ranging between 15–37.9% and 40–66.7% respectively. However, the fungal spores such as *Glomus* sp. (33.3%) and *Curvularia* sp. (20%) increased as compared to the preceded pollen zone BP–II.

Pollen Zone BP– IV (25–0 cm; 1.9 kyr B.P. to present)

The pollen assemblage (*Pinus–Cedrus–Picea–Abies–Alnus–Ulmus–Carpinus–Corylus–*Amaranthaceae–Caryophyllaceae–*Oldenlandia–* Tubuliflorae/Asteroideae –Liguliflorae/Cichorioideae) of the topmost zone has shown presence of a comparatively dense mixed coniferous/broad–leaved forest in the region. *Pinus* sp. (19.4–30.4% pollen), among the conifers of the arboreal taxa, is recorded in highest frequency (average ~26% pollen) in this pollen zone as compared to the preceding pollen zones. *Cedrus* sp. (4.8–13.2% pollen) followed *Pinus* sp. Other coniferous elements such as *Picea* sp. (0.2–2.1% pollen) and *Abies* sp. (1.4–8.3%) are recorded in low frequencies, but their values have increased as compared to the preceding pollen zones. *Podocarpus* sp. and *Tsuga* sp. have 0.3% and 0.8% pollen, thus, maintained their low record in this zone too. Among the broad–leaved taxa, *Alnus* sp. is recorded in moderate values (3.9–9.8%) and highest among the preceding zones. *Betula* sp. appeared for the first time with a very low pollen frequency (0.3–0.4%). However, other broad leaved taxa such as *Ulmus* sp. (1.4–7.9%), *Carpinus* sp. (1.2–6.1%), *Corylus* sp. (1.2–4.2%) are recorded in moderate to high frequencies although *Juglans* sp.(0.8–1.8% pollen) is noted with low value. *Croton* sp. shrubby taxon is recorded in sporadically in low values (0.3–0.4%).

Poaceae is recorded with low to moderate value (0.2–2.9%) as compared to the preceding pollen zones, whereas Cerealia shows a very low pollen frequency (0.5–2.7%) comparatively higher than the preceeded pollen zones (Fig. 8). Other cultural pollen taxa such as Amaranthaceae sp. (1–5.9%), Caryophyllaceae sp. (1.2–4.2%), Brassicaceae sp. (0.2–1.8%) and *Artemisia* sp. (2–3.7%) are recorded in moderate to high values. Tubuliflorae/ Asteroideae (2.9–11.8%) and other terrestrial herbs Liguliflorae/ Cichorioideae (0.7–32.7%), *Abutilon* sp. (average ~0.3%), *Aconitum* sp. (2.4–6.7%), *Oldenlandia* sp. (0.9–10%) have high and increased values relative to those in other pollen zones. *Saxifraga sibirica* , *Saxifraga* sp. and *Isopyrum* sp. appeared for the first time with low value of 0.3 to 0.4% , 0.3 to 0.5% and 0.35%, respectively. *Viola* sp. recorded a very low value (0.35%).

Polygonum lapthifolium (0.4–1.4%), *Polygonum hydopiper* (0.3–0.4%) and *Polygonum alatum* (0.4%) are the marshy taxa recorded in extremely low values.

Trilete fern spores decreased as compared to the preceding two pollen zones viz. zone II and zone III although higher than zone I and are recorded in good values (3.2–26.7%). However, monolete fern spores are represented in good values (7.3–37.9%) and almost maintained their frequencies as zone I and III but comparatively lower than Pollen zone II. The fungal spores such as *Glomus* sp. (2–82.8%) and *Nigrospora* sp. (3.2–22.2%) increased as compared to the preceded pollen zones. *Diploidea* sp. appears for the first time in this pollen zone with a moderate value of 3.2–5.5% while, *Curvularia* sp. (0.2–1%) records an extremely low value.

Inferences on pollen-based vegetation dynamics and associated climate change

Four phases of vegetation dynamics and associated climate change have been demarcated, based on the changes in the frequencies of especially the arboreal taxa (trees and shrubs) from the central Himalaya, India. The available pollen record, though poor, in the first phase (Pollen Zone BP–I) has revealed that between ~15.3 and 11.3 kyr B.P., *Pinus*-dominated open

Table S3. Sample identifier, depth, age, TOC, Stable carbon isotopic values (‰; VBDB), along with the low field magnetic susceptibility and LOI parameters.

Sample identifier	Depth (cm)	Age (ka)	TOC (%)	$\delta^{13}C$ (‰; VPDB)	Moisture (%)	Org-C (%)	CO_3 (%)	Norm. LF sus. (10^-8m^3kg-1)
BP 72 (top)	0	0.0	8.6	-27.6	2.87	20.28	1.49	0.451
BP 71	5	0.4	6.0	-28.1	8.35	13.91	1.51	0.663
BP 70	10	0.8	3.6	-27.3	1.92	9.92	2.12	0.739
BP 69	15	1.2	1.6	-25.7	1.07	4.54	1.70	0.368
BP 68	20	1.6	0.66	-25.5	0.88	2.88	1.36	0.354
BP 67	25	1.9	1.00	-25.1	0.60	3.96	1.49	0.475
BP66	30	2.1	0.30	-23.0	0.58	1.90	1.25	0.305
BP65	35	2.4	0.57	-23.1	0.83	2.27	1.91	0.285
BP64	40	2.7	0.22	-23.8	0.64	1.87	1.57	0.465
BP63	45	3.0	0.10	-23.8	0.33	1.09	1.12	0.280
BP62	50	3.3	0.52	-24.0	0.78	3.73	2.01	0.513
BP61	55	3.5	0.60	-23.9	1.72	5.50	2.24	0.787
BP60	60	3.7	0.50	-23.7	1.19	4.68	2.63	0.657
BP59	65	3.9	0.51	-23.4	1.05	4.62	2.56	0.611
BP58	70	4.1	0.46	-23.0	2.15	3.92	2.36	0.722
BP57	75	4.3	0.39	-22.9	1.87	2.85	2.20	0.422
BP56	80	4.5	0.46	-22.8	1.71	2.53	2.55	0.474
BP55	85	4.7	0.35	-22.9	1.52	3.18	1.94	0.448
BP54	90	4.9	0.26	-23.2	1.30	2.99	1.82	0.374
BP53	95	5.1	0.43	-23.0	0.64	5.19	1.88	0.491
BP52	100	5.3	0.30	-22.8	1.63	2.71	1.97	0.347
BP51	105	5.4	0.17	-22.9	1.54	1.76	2.11	0.324
BP50	110	5.6	0.17	-22.9	1.12	2.04	1.91	0.334
BP49	115	5.8	0.25	-22.9	1.39	2.22	1.80	0.315
BP48	120	6.0	0.19	-23.2	1.01	2.27	2.05	0.345
BP47	125	6.2	0.14	-22.2	1.14	2.06	2.19	0.391
BP46	130	6.4	0.17	-22.6	4.17	2.02	2.62	0.349
BP45	135	6.6	0.20	-23.2	3.00	2.22	2.16	0.322
BP44	140	6.8	0.21	-23.8	1.11	2.39	2.07	0.390
BP43	145	7.0	0.15	-23.8	1.40	1.92	2.14	0.511
BP42	150	7.2	0.20	-23.7	1.26	2.33	2.92	0.526
BP41	155	7.4	0.25	-24.1	1.92	2.66	3.88	0.650
BP40	160	7.6	0.30	-23.9	1.56	3.40	3.17	0.694
BP39	165	7.8	0.28	-24.0	5.93	2.85	2.64	0.620
BP38	170	7.9	0.10	-24.8	0.72	1.68	2.48	0.610
BP37	175	8.1	0.13	-24.2	1.10	2.26	3.36	0.582
BP36	180	8.2	0.24	-25.7	1.06	2.22	3.27	0.616
BP35	185	8.4	0.28	-25.2	1.26	2.92	2.40	0.474
BP34	190	8.5	0.25	-24.1	1.18	2.70	1.89	0.529
BP33	195	8.7	0.16	-26.7	1.06	1.15	1.15	0.277
BP32	200	8.8	0.10	-25.6	0.35	1.03	2.40	0.430
BP31	205	8.9	0.08	-26.9	0.59	0.62	1.54	0.281
BP30	210	9.1	0.09	-26.0	0.67	0.93	1.62	0.411
BP29	215	9.2	0.08	-26.2	0.35	1.44	2.60	0.447
BP28	220	9.4	0.10	-26.6	0.30	1.43	2.97	0.487
BP27	225	9.5	0.10	-26.7	3.96	1.06	2.79	0.450
BP26	230	9.7	0.17	-27.1	0.79	1.67	3.49	0.679
BP25	235	9.8	0.09	-27.1	0.26	0.87	2.06	0.491
BP24	240	10.0	0.10	-27.0	0.32	1.05	1.89	0.462
BP23	245	10.3	0.19	-26.9	0.76	1.87	3.70	0.721
BP22	250	10.5	0.16	-26.6	0.68	1.46	4.21	0.521
BP21	255	10.7	0.15	-26.3	1.30	1.29	4.08	0.502
BP20	260	10.9	0.35	-25.0	1.52	3.71	2.63	0.376
BP19	265	11.2	0.33	-24.7	1.76	4.04	2.37	0.405

BP18	270	11.4	0.29	-25.1	1.39	3.30	2.47	0.362
BP17	275	11.6	0.24	-25.2	1.52	3.04	2.85	0.394
BP16	280	11.9	0.21	-25.2	1.31	2.10	3.23	0.362
BP15	285	12.1	0.17	-25.3	2.12	2.59	2.12	0.299
BP14	290	12.3	0.10	-26.3	0.70	1.93	1.17	0.167
BP13	295	12.5	0.13	-26.6	0.59	1.57	1.22	0.283
BP12	300	12.8	0.15	-26.4	0.83	1.73	1.84	0.300
BP11	305	13.0	0.12	-25.7	0.80	1.50	2.82	0.343
BP10	310	13.2	0.13	-25.6	0.64	1.69	2.34	0.428
BP9	315	13.5	0.12	-25.6	0.67	1.85	2.05	0.352
BP8	320	13.7	0.14	-26.0	1.09	2.28	2.49	0.583
BP7	325	13.9	0.13	-24.7	0.83	2.13	2.75	0.562
BP6	330	14.1	0.16	-23.4	0.87	1.69	3.12	0.593
BP5	335	14.4	0.16	-25.6	0.88	1.97	2.85	0.671
BP4	340	14.6	0.14	-24.2	0.77	1.82	2.59	0.532
BP3	345	14.8	0.13	-25.3	0.57	1.49	2.59	0.627
BP2	350	15.0	0.10	-26.1	0.37	1.00	2.53	0.387
BP1 (Base)	355	15.3	0.13	-26.4	0.24	0.96	2.86	0.513

mixed coniferous (needle-leaved)/broad–leaved forest occupy the landscape around the study area under a relatively less cold and dry climate, probably indicating reduced monsoon precipitation. Subsequently, between ~11.3 and 4.9 kyr B.P. (Pollen Zone BP-II), savannah-type vegetation replaced the open mixed coniferous/broad-leaved forest, although *Pinus* continued to grow as a dominating taxon, under a cold and dry climate with relatively reduced monsoon precipitation. Between ~4.9 and 1.9 kyr B.P. (Pollen Zone BP-III), open mixed coniferous/broad-leaved forest was transformed into mixed coniferous/broad-leaved forest under a relatively warm climate with increased monsoon precipitation. Since ~1.9 kyr B.P. to the present (Pollen Zone BP-IV), further amelioration of climate took place as is manifested by a shift in the vegetation pattern. The dense mixed coniferous/broad–leaved forest came into being and replaced the mixed conifers/broad-leaved forest with the improvement and dominance of both the coniferous taxa,such as *Pinus*, *Cedrus*, *Abies* and *Picea*, as well as the broad-leaved taxa, such as *Alnus*, *Ulmus*, *Carpinus*, Juglans, *Corylus* and *Betula* under a relatively warmer climate, possibly indicating increased monsoon precipitation.

DISCUSSION

Monsoon reconstructions for the high altitude areas of Indian sub–continent are not only scarce, fragmentary, poorly resolved but also has poor chronometric control (Juyal *et al*., 2009). Selection of the appropriate proxy is another important restrictive factor in these areas as climatic conditions do not favor all the proxies. It is well established that the carbon isotope composition of SOM is determined by the in situ as well as catchment vegetation carbon isotope composition, which in turn depends on photosynthesis pathway of plants, as the different photosynthesis pathway i.e. C_3 and C_4 plants are characterized by different isotopic signature $\delta^{13}C_{org}$ values of C_3 plants range from −32 to −22‰ with average value of −26‰, and for C_4 plants it range from −16‰ to −10‰ with average value of −12.5‰ (Agrawal *et al.,* 2012; Basu *et al.,* 2015; Rao *et al.,* 2017). In the present study, the average $\delta^{13}C_{org}$ value of modern SOM is −25.9±0.9‰ (n=10). The average $\delta^{13}C_{org}$ values are falling within the range of $\delta^{13}C_{org}$ values of C_3 plants and indicate exclusive C_3 vegetation in this alpine meadow region. In addition, the $\delta^{13}C_{org}$ values of SOM from the profile shows large variation (5.9‰) from top to bottom and ranges between –28.1 and –22.2‰ with mean value of –24.1‰, further pointing out towards an exclusively C_3 vegetation in the study area during last ~15.3 kyr. On the basis of variation in the carbon isotope ($\delta^{13}C_{org}$), total organic carbon (TOC), magnetic susceptibility (χ_{lf}) and loss on ignition (LOI), eight climatic zones have been identified (Fig. 7). The independent environmental proxies used in this reconstruction are broadly in agreement with one another as well as with the local and regional reconstructions (Fig. 9). However, pollen analytical investigation could only provide four phases of vegetation dynamics and climate change. The middle part of the profile has not yielded sufficient pollen owing to the presence of various types of sand and sandy deposits between ~150–240 cm depths in the litho-column, producing a redox condition, wherein water becomes more oxygenated, which could hinder pollen preservation. Therefore, the possible reason for poor preservation may be downward particle transport through the water in coarser sediments (Ratmeyer e*t al.,* 1999) and the poor preservation in almost oxic sediments (Dupont and Wyputta, 2003). The morainal lakes are generally shallow and the poor preservation in such lakes following low lake level resulting from prolonged desiccation has also been observed (Kiage and Liu, 2009).

The detailed palaeo-vegetation and the ISM variability based on the multiproxy signals since ~15.3 kyr B.P. show prominent peaks in precipitation corresponding to the intensification of monsoon. At the bottom of the profile (~15.3 kyr B.P.), the $\delta^{13}C_{org}$ (–26.4‰) values are low, suggesting a warm and wet climate with an estimated precipitation of ~880 mm. A gradual increase in the isotopic values ($\delta^{13}C_{org}$= –23.4‰) imply that the conditions were becoming drier (~250 mm precipitation). This zone (~15.3–14.8 kyr B.P.) has sporadic representation of pollen, however the presence of conifers like *Pinus* are suggesting towards a drier climate. The presence of cultural pollen taxa such as Amaranthaceae, Caryophyllaceae, *Artemisia* sp., Brassicaceae sp., *Aconitum* sp. further indicate that the region was under the impact of cool and dry climate. Keeping in view the age

uncertainties, this phase broadly corresponds with the decline in the summer monsoon strength (16.5 and 14.5 kyr B.P.) reported from the nearest site at Goting, central Himalaya (Juyal *et al*., 2009). Sinha *et al*. (2005) have recorded a progressive lowering in oxygen isotope values between 15.2 and 14.3 kyr B.P. and attributed it to strengthening of summer monsoon intensity. Contrary to this, Juyal *et al.* (2009) believed that the data of Sinha *et al*., (2005) show an overall enrichment in ^{18}O between 15.5 and 14.7 kyr B.P. indicating a weak monsoon condition. Synthesis of palaeoclimatic records (different proxies) from the central Himalayan region also suggest a weaker phase of ISM (Fig. 9). This weak phase of ISM has also been interpreted as a phase of aridity between 15 and 13 kyr B.P. from the central Ganga plain (Sharma *et al*., 2004) and accords well with our results.

This phase (Zone I; ~15.3–14.8 kyr B.P.) although short-lived appears to be a transitional event during which the conditions changed from a wetter to one of the most prominent dry phases in central Himalaya. This dry phase is nested within the weakest ISM between 18.2 and 14.8 kyr B.P. (Rashid *et al*., 2011) and is consistent with the weak Asian monsoon resulting in the lowest precipitation in China as inferred from the Hulu, Donggee and Sanbao speleothem records (Wang *et al*. 2005, 2008) and other marine records (Rao *et al*., 2008, 2010;Staubwasser *et al*., 2002; Rassid *et al*., 2007, 2011, Thamban *et al*., 2011). The zone I of the present study also lies within the range of Heinrich event 1 (H1) and may be attributed to the southward migration, contraction, and/or intensity decrease of the ITCZ monsoonal rain belt (Deplazes *et al*., 2014). The arid conditions observed during this phase are in line with reconstructions from the Cariaco Basin (Peterson *et al*., 2000; Deplazes *et al*., 2013). This reduction in ISM is attributed to an abrupt increase in North Atlantic sea–ice extent. This increase in sea–ice extent results into a significant decrease in temperature all the way through the Northern Hemisphere, including the northern Indian Ocean and thereby delaying the onset of the ISM and resulting into a reducing of the ISM precipitation over the Indian subcontinent (Pausata *et al*., 2011).

Significant decresae of $\delta^{13}C_{org}$ values in Zone-II (14.8–14.2 kyr B.P.) reflect strengthening of the ISM intensity and is synchronous with the glacial–Bølling transition and advocate for a wet and warm climate. Further this zone has a fairly stable TOC and the organic content also does not show any significant changes. Palynological assemblage again shows sporadic pollen representation with some conifers and broad leaved taxa. The presence of monotele and fungal spore further support a warm and wet climate (Fig. 8). These inferences show very good correlation with other sites in the Himalaya as well as other parts of the Indian subcontinent (Fig. 9). Records of a gradual recovery of ISM has been reported from Goting, central Himalaya (Juyal *et al*., 2009), Tima cave (Sinha *et al*., 2005), Chandra tal (Rawat *et al.,* 2015) and Ladakh (Bhattacharyya, 1989; Demske *et al.,* 2009). More recently, lower $\delta^{18}O$ values at ~15 and 13.5 kyr B.P. from the Krem Mawmluh cave; have been ascribed to increased monsoon strength around the Bølling–Allerød (Huguet *et al.,* 2018). The abrupt changes in ISM have been ascribed to the alterations in temperature gradients that affected the wind circulation patterns over the Bay of Bengal and northeast India (Huguet *et al.,* 2018).

Zone–III (~14.2–12.1 kyr B.P.) is characterized by a prominent increase of $\delta^{13}C_{org}$ values (–25.5‰) with respect to zone II and relatively low TOC content. Pollen is again sporadically represented and do not provide any significant inferences. The overall trend of the proxies and sparse vegetation cover indicate a phase of weak precipitation resulting into a drier climate. It is important to notice that the later phase of this broadly corresponds to the Younger Dryas (YD) cold event (Bond *et al*., 1993; Adams *et al*., 1999; Alley, 2000). Palaeoclimatic reconstructions from Garbayang basin (central Himalaya) show an abrupt drop in susceptibility, S–ratio and concentration of basic oxides during ~12–11 kyr B.P., and has been attributed to the YD (Juyal *et al*., 2009). Similar responses attributed to the YD have been reported from Chandra Tal, western Himalaya (Rawat *et al*., 2015), Dokriani valley, Central Hamalaya (Bhattacharyya *et al*., 2011), central Himalaya (Pant *et al*., 2005) and core monsoon zone of India (Quamar and Chauhan, 2012; Quamar and Bera, 2017). The records of YD cooling event are regionally well recorded in the cave deposits like Timta Cave (YD – 12.7 and 11.6 cal kyr B.P.) Kumaun Himalaya (Sinha *et al*., 2005), ~Hulu cave (12,823 to 11,473 cal yrs B.P.) Tang Shan in eastern China (Cheng *et al*., 2006), Dongge cave (~1,2850 to 11,560 cal yrs B.P.), south east China (Dykoski *et al*., 2005) as well as from the marine records of Arabian sea and Bay of Bengal (Schultz *et al*., 1998; Kudrass *et al*., 2001; Gupta *et al*., 2003, 2005, 2013). All these studies have suggested that during the YD, the Indian subcontinent has witnessed cold–dry climate and a weak ISM. The weakening of ISM during YD is attributed to the weakening of the Atlantic Meridional Overturning Circulation (McManus *et al*., 2004). Our rainfall reconstruction also shows a decreased precipitation of ~440 mm during ~14.2–12.1 kyr B.P. (Fig. 7). However, having a look at the whole reconstructed data, it is noted that this phase has not been the driest phase during the last ~15.3 kyr B.P. We propose that during the YD, the study area was getting winter precipitation from the mid–latitude westerlies. The cold temperature and the influence of high winter Westerly flow in the region during YD (Rawat *et al.,* 2015) should have produced hostile conditions for glacier advances and is accordingly reported from the adjoining Dunagiri valley (Sati *et al.,* 2014).

This phase (Zone–IV; ~12.1–8.5 kyr B.P.) is marked by a gradual decline in the $\delta^{13}C_{org}$ values and an overall increase in the magnetic susceptibility, suggesting a wetter climate (max. precipitation of ~1150 mm). The wetter conditions are attributed to gradual strengthening of the ISM after the post glacial cooling event (YD) (Fig. 7). Similar inferences have been made from adjacent Malari palaeolake site with a strengthened monsoon conditions soon after 12 ka (Srivastava *et al.,* 2013). Recently, Bhushan *et al*. (2018) have also reported a gradual strengthening of the ISM (humid conditions) on the basis of detrital proxies from a nearby site in central Himalaya. The early Holocene strengthening of ISM has been confirmed regionally and our data correlates well with these studies established (Fig. 9). For example, on the basis of lower $\delta^{18}O$ values of Ostracods and calcium carbonate deposits, Dixit *et al*. (2014) proposed a strengthening of ISM during the early Holocene (~11–9.4 kyr B.P.) from Raiwasa lake NW India. More importantly, the post YD strengthening of ISM has been documented in both marine and terrestrial proxies on regional scale (Ponton *et al*., 2012; Dutt *et al*., 2015; Dixit *et al*., 2014; Kessarkar *et al.,* 2013; Govil and Naidu, 2011; Wang *et al.,* 2001; Fleitmann *et al*., 2003; Overpeck *et al*., 1996; Sirocko *et al*., 1993). The early Holocene monsoon intensification in the south Asian monsoon system has been ascribed to two inherently related different processes that is

boreal summer insolation, which is considered to be an external forcing mechanism (Overpeck *et al*., 1996; Kutzbach and Street–Perrott, 1985) and a significant reduction in albedo (reflection of solar radiation) due to decrease in Tibetan Plateau snow cover (Marzin and Braconnot, 2009). Besides this, the northward migration of the Inter Tropic Convergence Zone (ITCZ) has been reported (10.3–9.6 kyr B.P.) to be a reason for this increase in the early Holocene ISM precipitation (Burns *et al*., 1998; Fleitmann *et al*., 2003).

A gradual increase in the isotopic values ($\delta^{13}C_{org}$ = –22.8‰) continued through this phase (Zone–V). Our data suggest that the area was experiencing dry climate conditions that must have been driest at ~6 kyr B.P. Detrital proxies data from a nearby site, which is located in ISM dominated central Himalaya, suggested a moderate precipitation condition between ~8,600 and 5,800 cal yrs B.P. (Bhushan *et al*., 2018). Similarly, Rawat *et al*. (2015) reported water stress condition from the Chandra valley during ~8,810–6,732 cal yrs B.P. Studies from central Himalaya also suggest a cold and dry climate during 8,300–6,000 cal yrs B.P. (Bali *et al.*, 2015; Kotlia *et al*., 2010; Ranhotra *et al*., 2001; Phadtare, 2000). Our study is in agreement with these observations; however, our reconstructed precipitation data shows that this was the driest period in last ~15.3 kyr. This significant dryness during the mid–Holocene is attributed to a weak ISM and the location of study area in a rain shadow zone. We infer this since the study area is located on the boundary of ISM influence (transition zone) therefore any change in the ISM intensity will get an amplified signal here.

Enrichment in the isotopic values with a slight depletion towards the end of this phase (Zone–V; ~8.8–6.0 kyr B.P.), a higher TOC, and low magnetic susceptibility suggest an overall drier condition with progressive improvement towards the termination of this zone. The continuation of the drier climate is attributed to weak ISM that is reported from other sites from the central Himalaya (Bhushan *et al*., 2018 and references therein; Fig. 9). The declining ISM and the onset of regional aridity have been ascribed for the collapsing Indus valley civilization (Possehl, 1997; Gupta *et al.,* 2003; Dixit *et al*., 2014). According to Chauhan (2000), cool and dry conditions with an ameliorating condition existed in the central India (Chattisgarh) during ~6500–4250 yrs B.P. The decreasing trend in the rainfall pattern post ~6 kyr B.P. is attributed to the progressive decrease in insolation and south ward shift of the ITCZ after mid–Holocene. After ~4 kyr B.P. a slight decrease followed by increase in the isotopic values is reported. During this period the carbonate and magnetic susceptibility also shows decrease in their values. This trend of the proxies suggests a slight betterment followed by a deteriorating climate condition under a week ISM regime. The presence of conifers like *Pinus*, *Cedrus* etc. towards the top of this zone further suggest a dry climate. However, it is also observed that the boundary of this phase where the trend of all the proxies is changing show the emergence of broad leaved taxa hinting towards climate amelioration. Our data suggests a weak ISM during this phase and has a broad local as regional correlation (Bhushan *et al*., 2018; Rawat *et al*., 2015; Ruhland *et al*., 2006; Pant *et al*., 2005; Ranhotra and Bhattacharyya, 2010; Bali *et al*., 2015; Bali *et al*., 2017).

The period between ~2 kyr B.P. and present is marked by gradually lowering of $\delta^{13}C_{org}$ values. The increasing trend in organic carbon and high magnetic susceptibility again indicates warmer and wetter phases of climate. During this phase highest values of precipitation has been recorded (with a max. of ~1746 mm). Further, appearance of broad-leaved taxa viz. *Alnus*, *Ulmus*, *Carpinus*, *Corylus* and sporadically represented *Betula* for the first time in the pollen count indicates a warm and moist climate. This phase marks the revival of good summer monsoon after a long break period during the mid–Holocene. Recently, Bhushan *et al*. (2018) suggested that after ~1.8 kyr B.P. the hydrological conditions in the central Himalaya improved and have correlated this to the anomalous Medieval Warm Period (Lamb, 1965) and advocated a regional representation of this warming trend as phase is being reported from various parts of the Himalaya. Rawat *et al*. (2015) and Ruhland *et al*. (2006) from western and central Himalaya have also reported an overall moist climate during the last 2 kyr B.P., punctuated by small dry spell during the LIA. The strengthening of the ISM after ~2 kyr B.P. is regionally reported in many studies for example from Himalaya (Kar *et al.*, 2002; Ranhotra and Bhattacharyya, 2010; Bali *et al*., 2015; Bali *et al*., 2017; Kotlia *et al*., 2015; Sanwal *et al.*, 2013; Shekhar *et al*., 2018) and from central India (Chauhan, 2000; Chauhan and Quamar, 2012; Quamar and Nautyal, 2017; Quamar and Bera, 2017). Further our data is in compliance with other studies from this region that suggest wetter conditions during at least certain parts of the LIA (Denniston *et al*., 2000; Cook *et al*., 2003; Yadav and Singh, 2002; Rühland *et al*., 2006; Kotlia *et al*., 2012). However, the wetter LIA is attributed to the mid–latitude westerlies that were strong during this time.

CONCLUSIONS

The present study from a climatologically important site that lies at the northern boundary of the ISM in central Himalaya has given some important insights on the monsoon variability during lat ~15.3 kyr. The multiproxy studies, precipitation reconstruction supported by luminescence ages indicate three dry and wet phases of climate. The first phase of dryness (~15.3–14.8 kyr B.P.) has been interpreted as arid phase from other nearby localities and ascribed as weaker phase of ISM, which was followed by a normal phase of monsoon that showed improvement after ~14.8–14.2 kyr B.P. A drier period corresponding to the global YD has been recorded between ~14 and 12 kyr B.P., followed by a gradual strengthening in the ISM. The post YD strengthening of ISM is regionally reported and has been ascribed to boreal summer insolation, reduction in albedo and northward migration of the Inter Tropic Convergence Zone. Mid– Holocene has been suggested to be a period of weak to moderate ISM in the central Himalaya. Our data shows that this was the driest phase during the last ~15 kyr in our study area. We infer that during YD our area was getting precipitation from the mid–latitude westerlies that are suggestive to be active during this time. The driest mid–Holocene is a response of weak ISM as well as mid–latitude westerlies. The late–Holocene strengthening of ISM is a regional phenomenon suggesting a close link between the ISM and higher Himalayan climate. We infer that proxy response is a function of sensitivity of study site to climatic domain and in order to understand the coupled influence of mid–latitude westerlies and the ISM studies need to be carried out in locations that are lying in the transition of these two weather systems.

ACKNOWLEDGMENTS

The authors are thankful to the Director, Birbal Sahni Institute of Palaeosciences, Lucknow, India for providing

laboratory facilities. This work was carried out with financial support from the Department of Science and Technology (DST), Government of India, India (Ref: No. SR/FTP/ES–23/2013). We thank Dr. A. D. Shukla for providing dose rate of OSL samples. Authors are grateful to the editor and anonymous reviewer for their valuable suggestions and constructive comments, which helped us improve the manuscript.

REFERENCES

Adamiec, G. and Aitken, M. J. 1998. Dose–rate conversion factors: update. Ancient TL, **16**: 37–50.

Adams, J., Maslin, M. and Thomas, E. 1999. Sudden climate transitions during the Quaternary. *Progress in Physical Geography*, **23**(1): 1–36.

Ali, S. N. and Juyal, N. 2013. Chronology of late quaternary glaciations in Indian Himalaya: a critical review. *Journal Geological Society of India,* **82**: 628–638.

Ali, S. N., Dubey, J., Ghosh, R., Quamar, M. F., Sharma, A., Morthekai, P., Dimri, A. P., Shekhar, M., Arif, M. and Agrawal, S. 2018. High frequency abrupt shifts in the Indian summer monsoon since Younger Dryas in the Himalaya. *Scientific Reports,* **8**: 9287.

Ali, S. N., Dubey, J., Shekhar, M. and Morthekai, P. 2019. Holocene Indian Summer Monsoon variability from the core monsoon zone of India, a pollen-based review. *Grana,* **58**: 311–327.

Ali, S. N., Agrawal, S., Sharma, A., Phartiyal, B., Morthekai, P., Govil, P., Bhushan, R., Farooqui, S., Jena, P. S. and Shivam, A. 2020a. Holocene hydroclimatic variability in the Zanskar Valley, Northwestern Himalaya, India. *Quaternary Research* (*in press*).

Ali, S. N., Quamar, M. F., Dubey, J., Morthekai, P., Bisht, P., Pandey, P., Shekhar, M. and Ghosh, R. 2020b. Surface pollen distribution in an alpine zone of the higher Himalaya: a case study from the Kalla glacier valley, India. *Botany Letters* (*in press*).

Alley, R. B. 2000. The Younger Dryas cold interval as viewed from central Greenland. *Quaternary science reviews*, **19**(1-5): 213–226.

Bali, R., Ali, S. N., Bera, S. K., Patil, S. K., Agarwal, K. K., Nautiyal, C. M. 2015. Holocene Climatic Changes on Central Indian Himalayan (Glaciers), pp. 467–471. In: Impact of Anthropocene vis–a–vis. (Ed. Lollino, G.) Eng. Geol. for Soc. and Territ. 1. Springer Int. Pub. Switzerlan.

Bali, R., Chauhan, M. S., Mishra, A. K., Ali, S.N., Tomar, A., Khan, I., Singh, D. S. and Srivastava, P. 2017. Vegetation and climate change in the temperate–subalpine belt of Himachal Pradesh since 6300 cal. yrs. BP, inferred from pollen evidence of Triloknath palaeolake. *Quaternary International,* **444**: 11–23.

Banerjee, D., Murray, A. S., Bøtter–Jensen, L. and Lang, A. 2001. Equivalent dose estimation using a single aliquot of polymineral fine grains. *Radiation Measurement,* **33**: 73–94.

Banerji, U. S., Arulbalaji, P., Padmalal, D. 2020. Holocene climate variability and Indian Summer Monsoon: An overview. *The Holocene*, 1–30. doi.org/10.1177/0959683619895577.

Basu, S., Agrawal, S., Sanyal, P., Mahato, P., Kumar, S. and Sarkar, A. 2015. Carbon isotopic ratios of modern C3–C4 plants from the Gangetic Plain, India and its implications to paleovegetational reconstruction. *Palaeogeography, Palaeoclimatology, Palaeoecology,* **440**: 22–32.

Basu, S., Sanyal, P., Pillai, A. A. S. and Ambili, A. 2019. Response of grassland ecosystem to monsoonal precipitation variability during the Mid-Late Holocene: Inferences based on molecular isotopic records from Banni grassland, western India. *PloS one,* **14:** e0212743.

Bates, R. L. and J. A. Jackson. 1984. Dictionary of Geological Terms, 3rd edition. American Geological Institute, 571pp.

Bengtsson, L. and Enell, M. 1986. Chemical analysis, pp. 423–451. In: Handbook of Holocene palaeoecology and palaeohydrology (Ed., Berglund, B.E.) Chichester: John Wiley.

Bhattacharayya, A., Ranhotra, P. S. and Gergan, J. T. 2011. Vegetation vis–a–vis climate and glacier history during 12,400 to 5,400 yr BP from Dokriani valley, Garhwal Himalaya, India. *Journal Geological Society of India,* **77**: 401– 408.

Bhattacharyya, A. 1989. Vegetation and climate during the last 30,000 years in Ladakh. *Palaeogeography Palaeoclimatology Palaeoecology,* **73**: 25–38.

Bhushan, R., Sati, S. P., Rana, N., Shukla, A. D., Mazumdar, A. S. and Juyal, N. 2018. High–resolution millennial and centennial scale Holocene monsoon variability in the Higher Central Himalayas. *Palaeogeography Palaeoclimatology Palaeoecology,* **489**: 95–104.

Birks, H. H. and Birks, H. J. B. 2006. Multi-proxy studies in palaeolimnology. *Vegetation History and Archaeobotany,* **15**: 235–51.

Bisht, P., Ali, S. N., Shukla, A.D., Negi, S., Sundriyal, Y. P., Yadava, M. G. and Juyal, N. 2015. Chronology of late Quaternary glaciation and landform evolution in the upper Dhauliganga valley, (Trans Himalaya), Uttarakhand, India. *Quaternary Science Reviews,* **129**: 147–162.

Bookhagen, B. and Burbank, D. W. 2006. Topography, relief, and TRMM–derived rainfall variations along the Himalaya. *Geophysical Research Letters,* **33**: L08405, doi:10.1029/2006GL026037.

Bookhagen, B. and Strecker, M. R. 2008. Orographic barriers, high-resolution TRMM rainfall, and relief variations along the eastern Andes. *Geophysical Research Letters,* **35**: L06403, doi:10.1029/2007GL032011.

Bond, G., Broecker, W. S., Johnson, S., McManus, J., Labeyrie, L., Jouzel, J. and Bonani, G. 1993. Correlations between climate records from North Atlantic sediments and Greenland ice. *Nature*, **365**: 143–147.

Bøtter–Jensen, L., Thomsen, K. J. and Jain, M. 2010. Review of optically stimulated luminescence (OSL) instrumental developments for retrospective dosimetry. *Radiation Measurement,* **45**: 253–257.

Burns, S. J., Matter, A., Frank, N. and Mangini, A. 1998. Speleothem–based paleoclimate record from northern Oman. *Geology,* **26**: 499–502.

Cerling, T. E. 1992. Use of carbon isotopes in paleosols as an indicator of the P (CO2) of the paleoatmosphere. *Global Biogeochemical Cycles,* **6**: 307–314.

Champion, H. G. and Seth, S. K. 1968. A Revised Survey of the Forest Types of India. Government of India Press, Delhi, 404 pp.

Chandel, H. N., Patel, A. D., Vaghela, H. R. and Ubale, G. P. 2006. An effective and reuseable sampling pipe for luminescence dating. *Ancient TL,* **24**: 21–22

Chauhan, M. S. 2000. Pollen evidence of late–quaternary vegetation and climate change in Northeastern Madhya Pradesh, India. *Paleobotanist,* **49**: 491–500.

Chauhan, M. S. and Quamar, M. F. 2012. Pollen records of vegetation and inferred climate change in southwestern Madhya Pradesh during the last ca. 3800 years. *Journal of the Geological Society of India,* **80**(4): 470–480.

Cheng, H., Edwards, R. L., Wang, Y., Kong, X., Ming, Y., Kelly, M. J., Wang, X., Gallup, C. D. and Liu, W. 2006. A penultimate glacial monsoon record from Hulu Cave and two-phase glacial terminations. *Geology*, **34**(3): 217–220.

Cook, E. R., Anchukaitis, K. J., Buckley, B. M., D'Arrigo, R. D., Jacoby, G. C. and Wright, W. E. 2010. Asian monsoon failure and megadrought during the last millennium. *Science,* **328**: 486–489.

Dean, W. E. 1974. Determination of carbonate and organic matter in calcareous sediments and sedimentary rocks by loss on ignition; comparison with other methods. *Journal of Sedimentary Research,* **44**: 242–248.

Denniston, R. F., González, L. A., Asmerom, Y., Sharma, R. H. and Reagan, M. K. 2000. Speleothem evidence for changes in Indian summer monsoon precipitation over the last Demske 2300 years. *Quaternary Research,* **53:** 196–202.

Deplazes, G., Lückge, A., Peterson, L. C., Timmermann, A., Hamann, Y., Hughen, K. A., Röhl, U., Laj, C., Cane, M. A., Sigman, D. M. and Haug, G. H. 2013. Links between tropical rainfall and North Atlantic climate during the last glacial period. *Nature Geoscience,* **6**: 213–217.

Deplazes, G., Lückge, A., Stuut, J–B. W., Pätzold, J., Kuhlmann, H., Husson D., Fant, M. and Haug, G. H. 2014. Weakening and strengthening of the Indian monsoon during Heinrich events and Dansgaard–Oeschger oscillations, *Paleoceanography,* **29**: 99–114. doi:10.1002/2013PA002509.

Diefendorf, A. F., Mueller, K. E., Wing, S. L., Koch, P. L. and Freeman, K. H. 2010. Global patterns in leaf ^{13}C discrimination and implications for studies of past and future climate. *Proceedings of the National Academy of Science,* USA, **107**: 5738–5743.

Dixit, Y., Hodell, D. A. and Petrie, C. A. 2014. Abrupt weakening of the summer monsoon in northwest India ~4100 yr ago. *Geology,* **42**: 339–342.

Dubey, J., Ghosh, R., Agrawal, S., Quamar, M. F., Morthekai, P., Sharma, R. K., Sharma, A., Pandey, P., Srivastava, V. and Ali, S. N. 2018. Characteristics of modern biotic data and their relationship to vegetation of the Alpine zone of Chopta valley, North Sikkim, India: Implications for palaeovegetation reconstruction. *The Holocene,* **28**: 363–376.

Dupont, L. M., and Wyputta, U. 2003. Reconstructing pathways of aeolian pollen transport to the marine sediments along the coastline of SW Africa. *Quaternary Science Review,* **22**: 157–174.

Demske, D., Tarasov, P. E., Wünnemann, B. and Riedel, F. 2009. Late glacial and Holocene vegetation, Indian monsoon and westerly circulation in the Trans-Himalaya recorded in the lacustrine pollen sequence from Tso Kar, Ladakh, NW India. *Palaeogeography, Palaeoclimatology, Palaeoecology*, **279**(3-4): 172–185.

Dutt, S., Gupta, A. K., Clemens, S. C., Cheng, H., Singh, R. K., Kathayat, G. and Edwards, R. L. 2015. Abrupt changes in Indian summer monsoon strength during 33,800 to 5500 years BP. *Geophysical Research Letters*, **42**: 5526–5532.

Dykoski, C. A., Edwards, R. L., Cheng, H., Yuan, D., Cai, Y., Zhang, M., Lin, Y., Qing, J., An, Z. and Revenaugh, J. 2005. A high–resolution, absolute–dated Holocene and deglacial Asian monsoon record from Dongge Cave, China. *Earth and Planetary Science Letters,* **233**: 71–86.

Ekart, D. D., Cerling, T. E., Montañez, I. P. and Tabor, N. J. 1999. A 400 million year carbon isotope record of pedogenic carbonate: implications for paleoatmospheric carbon dioxide. *American Journal of Science,* **299**: 805–827.

Erdtman, G. 1945. Pollen Morphology and Plant Taxonomy. IV. Svensk. Bot. Tidskr, **39**: 279–285. Wiksell, Stockholm, Sweden.

Faegri, K. and Iversen. J. 1989. Textbook of pollen analysis, Fourth edition. John Wiley and Sons, Chichester, UK.

Finkel, R. C., Owen, L. A., Barnard, P. L. and Caffee, M. W. 2003. Beryllium–10 dating of Mount Everest moraines indicates a strong monsoon influence and glacial synchroneity throughout the Himalaya. *Geology,* **31**: 561–564.

Fleitmann, D., Burns, S. J., Mudelsee, M., Neff, U., Kramers, J., Mangini, A. and Matter, A. 2003. Holocene forcing of the Indian monsoon recorded in a stalagmite from southern Oman. *Science,* **300:** 1737–1739.

Fu, C. 1992. Transitional climate zones and biome boundaries: a case study from China, pp. 394–402. In: Landscape Boundaries. Springer, (Eds. Hansen, A.J. and Castri, F.D.), Verlag, New York.

Gadgil, S. 2006. The Indian Monsoon, GDP and agriculture. *Economic and Political Weekly,* **41:** 4887–4895.

Galbraith, R. F., Roberts, R. G., Laslett, G. M., Yoshida, H. and Olley, J. M. 1999. Optical dating of single and multiple grains of quartz from Jinmium rock shelter, northern Australia: part I, experimental design and statistical models. *Archaeometry*, **41** (2): 339–364.

Govil, P. and Naidu, P. D. 2011. Variations of Indian monsoon precipitation during the last 32 kyr reflected in the surface hydrography of the Western Bay of Bengal. *Quaternary Science Reviews,* **30:** 3871–3879.

Grimm, E. 1990. Tilia, tiliagraph and tiliaview. PC Spreadsheat and Graphics Software for Pollen Data. Illinois State Museum, IL, USA.

Gupta, A. K., Anderson, D. M. and Overpeck, J. T. 2003. Abrupt changes in the Asian southwest monsoon during the Holocene and their links to the North Atlantic Ocean. *Nature,* **421:** 354–356.

Gupta, A. K., Das, M. and Anderson, D. M. 2005. Solar influence on the Indian summer monsoon during the Holocene. *Geophysical Research Letters,* **32:** L17703, doi:10.1029/2005GL022685.

Gupta, A. K., Mohan, K., Das, M. and Singh, R. K. 2013. Solar forcing of the Indian summer monsoon variability during the Ållerød period. *Scientific Reports,* **3**: 2753. DOI: 10.1038/srep02753.

Gupta, H. P. and Sharma, C. 1986. Pollen flora of north–west Himalaya. Lucknow: Indian Association of Palynostratigraphers–illus. *En Icones, Palynology, Keys. Geog,* **6**: 181pp.

Harris, I., Jones, P. D., Osborn, T. J. and Lister, D. H. 2014. Updated high–resolution grids of monthly climatic observations e the CRU TS 3.10. *International Journal of Climatology,* **34:** 623–642.

Hatté, C., Antoine, P., Fontugne, M., Lang, A., Rousseau, D. D. and Zöller, L. 2001. $\delta^{13}C$ of loess organic matter as a potential proxy for paleoprecipitation. *Quaternary Research,* **55:** 33–38.

Heiri, O., Lotter, A. F. and Lemcke, G. 2001. Loss on ignition as a method for estimating organic and carbonate content in sediments: reproducibility and comparability of results. *Journal of Paleolimnology,* **25:** 101–110.

Herzschuh, U. 2006. Palaeo-moisture evolution in monsoonal Central Asia during the last 50,000 years. *Quaternary Science Reviews,* **25:** 163–178.

Huguet, C., Routh, J., Fietz, S., Lone, M. A., Kalpana, M. S., Ghosh, P., Mangini, A., Kumar,V. and Rangarajan, R. 2018. Temperature and Monsoon Tango in a Tropical Stalagmite: Last Glacial Interglacial Climate Dynamics. *Scientific Reports,* **8**: 5386, doi:10.1038/s41598–018–23606–w.

Jensen, E. S. 1991. Evaluation of automated analysis of 15 N and total N in plant material and soil. *Plant and soil*, **133**(1): 83–92.

Juyal, N., Pant, R. K., Basavaiah, N., Bhushan, R., Jain, M., Saini, N. K., Yadava, M. G. and Singhvi, A. K. 2009. Reconstruction of Last Glacial to early Holocene monsoon variability from relict lake sediments of the Higher Central Himalaya, Uttrakhand, India. *Asian Earth Science,* **34:** 437–449.

Kar, R., Ranhotra, P. S., Bhattacharyya, A. and Sekar, B. 2002. Vegetation vis–à–vis climate and glacial fluctuations of the Gangotri Glacier since the last 2000 years. *Current Science,* **82:** 347–351.

Kessarkar, P. M., Purnachadra Rao, V., Naqvi, S. W. A. and Karapurkar, S. G. 2013. Variation in the Indian summer monsoon intensity during the Bølling-Ållerød and Holocene. *Paleoceanography and Paleoclimatology,* **28:** 413–425.

Kiage, L. M. and Liu, K. B. 2009. Palynological evidence of climate change and land degradation in the Lake Baringo area, Kenya, East Africa, since AD 1650. *Palaeogeography, Palaeoclimatology, Palaeoecology*, **279**(1-2): 60–72.

Kohn, M. J. 2010. Carbon isotope compositions of terrestrial C3 plants as indicators of (paleo) ecology and (paleo) climate. *Proceedings of the National Academy of Science,* USA. **107:** 19691–19695.

Kotlia, B. S., Ahmad, S. M., Zhao, J. X., Raza, W., Collerson, K. D., Joshi, L. M. and Sanwal, J. 2012. Climatic fluctuations during the LIA and post–LIA in the Kumaun Lesser Himalaya, India: evidence from a 400 y old stalagmite record. *Quaternary International,* **263:** 129–138.

Kotlia, B. S., Sanwal, J., Phartiyal, B., Joshi, L. M., Trivedi, A. and Sharma, C. 2010. Late Quaternary climatic changes in the eastern Kumaun Himalaya, India, as deduced from multi–proxy studies. *Quaternary International,* **213:** 44–55.

Kotlia, B. S., Singh, A. K., Joshi, L. M. and Dhaila, B. S. 2015. Precipitation variability in the Indian Central Himalaya during last ca. 4,000 years inferred from a speleothem record: Impact of Indian Summer Monsoon (ISM) and Westerlies. *Quaternary International,* **371**: 244–253.

Kudrass, H. R., Hofmann, A., Doose, H., Emeis, K. and Erlenkeuser, H. 2001. Modulation and amplification of climatic changes in the Northern Hemisphere by the Indian summer monsoon during the past 80 ky. *Geology,* **29**: 63–66.

Kutzbach, J. E. and Street–Perrott, F. A. 1985. Milankovitch forcing of fluctuations in the level of tropical lakes from 18 to 0 kyr BP. *Nature,* **317**: 130.

Lamb, H. H. 1965. The early medieval warm epoch and its sequel. *Palaeogeography Palaeoclimatology Palaeoecology,* **1**: 13–37.

Leipe, C., Demske, D. and Tarasov, P. 2014. A Holocene pollen record from the northwestern Himalayan lake Tso Moriri: implications for palaeoclimatic and archaeological research. *Quaternary International,* **348**: 93–112.

Marzin, C. and Braconnot, P. 2009. Variations of Indian and African monsoons induced by insolation changes at 6 and 9.5 kyr BP. *Climate Dynamics,* **33:** 215–231.

McManus, J. F., Francois, R., Gherardi, J. M., Keigwin, L. D. and Brown–Leger, S. 2004. Collapse and rapid resumption of Atlantic meridional circulation linked to deglacial climate changes. *Nature,* **428**: 834. doi: 10.1038/*Nature,*02494

Meyer, M. C., Hofmann, C. C., Gemmell, A. M., Haslinger, E., Häusler, H. and Wangda, D. 2009. Holocene glacier fluctuations and migration of Neolithic yak pastoralists into the high valleys of northwest Bhutan.

Quaternary Science Reviews, **28**: 1217–1237.

Moore, P. D., Webb, J. A. and Collinson. M. E. 1991. Pollen analysis, Second edition. Blackwell Scientific Publications, Oxford, UK.

Morthekai, P. and Ali, S. N. 2014. Luminescence dating using quartz – for end–users. *Gondwana Geological Magzine,* **29:** 1–10.

Murray, A. S. and Wintle, A. G. 2000. Luminescence dating of quartz using an improved single aliquot regenerative–dose protocol. *Radiation Measurement,* **32:** 57–73.

National Research Council 2005. The Geological Record of Ecological Dynamics—Understanding the Biotic Effects of Future Environmental Change. National Academies Press, Washington, DC.

Overpeck, J., Anderson, D., Trumbore, S. and Prell, W. 1996. The southwest Indian monsoon over the last 18,000 years. *Climate Dynamics,* **12:** 213–225.

Oldfield, F., Barnosky, C., Leopold, E. B. and Smith, J. P. 1983. Mineral magnetic studies of lake sediments. *Paleolimnology*. Springer, Dordrecht 37–44.

Parnell, A. 2016. Bchron: Radiocarbon dating, age–depth modelling, relative sea level rate estimation, and non–parametric phase modelling. *R package version 4.1.1*. http://CRAN.R–project.org/package=Bchron.

Pausata, F. S., Battisti, D. S., Nisancioglu, K. H. and Bitz, C. M. 2011. Chinese stalagmite δ 18 O controlled by changes in the Indian monsoon during a simulated Heinrich event. *Nature Geosciences,* **4**: 474.

Peterson, L. C., Haug, G. H., Hughen, K. A. and Röhl, U. 2000. Rapid changes in the hydrologic cycle of the tropical Atlantic during the last glacial. *Science,* **290**: 1947–1951.

Phadtare, N. R. 2000. Sharp decrease in summer monsoon strength 4000–3500 cal yr BP in the Central Higher Himalaya of India based on pollen evidence from alpine peat. *Quaternary Research,* **53**:122–129.

Ponton, C., Giosan, L., Eglinton, T. I., Fuller, D. Q., Johnson, J. E., Kumar, P. and Collett, T. S. 2012. Holocene aridification of India. *Geophysical Research Letters,* **39:** L03704.

Pant, R. K., Phadtare, N. R., Chamyal, L. S. and Juyal, N. 2005. Quaternary deposits in Ladakh and Karakoram Himalaya: a treasure trove of the palaeoclimate records. *Current Science*, **88**: 1789–1798.

Possehl, G. L. 1997. The transformation of the Indus civilization. *Journal of World Prehistory,* **11**(4): 425–472.

Prasad, S. and Enzel, Y. 2006. Holocene paleoclimates of India. *Quaternary Research,* **66:** 442–453.

Prasad, S., Anoop, A., Riedel, N., Sarkar, S., Menzel, P., Basavaiah, N., Krishnan, R., Fuller, D., Plessen, B., Gaye, B. and Röhl, U. 2014. Prolonged monsoon droughts and links to Indo–Pacific warm pool: a Holocene record from Lonar Lake, central India. *Earth and Planetary Science Letters,* **391:** 171–182.

Prescott, J. R. and Hutton, J. T. 1994. Cosmic ray contributions to dose rates for luminescence and ESR dating: large depths and long–term time variations. *Radiation Measurement,* **23:** 497–500.

Quamar, M. and Chauhan, M. S. 2012. Late Quaternary vegetation, climate as well as lake–level changes and human occupation from Nitaya area in Hoshangabad district, southwestern Madhya Pradesh (India), based on pollen evidence. *Quaternary International,* **263:** 104–113.

Quamar, M. F. and Bera, S. K. 2017. Pollen records related to vegetation and climate change from northern Chhattisgarh, central India during the late Quaternary. *Palynology,* **41:** 17–23.

Quamar, M. F. and Nautiyal, C. M. 2017. Mid–Holocene pollen records from southwestern Madhya Pradesh, central India, and their palaeoclimatic significance. *Palynology,* **41:** 401–411.

Rana, N., Bhattacharya, F., Basavaiah, N., Pant, R. K. and Juyal, N. 2013. Soft sediment deformation structures and their implications for late quaternary seismicity on the south tibetan detachment system, central Himalaya (Uttarakhand), India. *Tectonophysics,* **592:** 165–174.

Rana, N., Sharma, S., Ali, S. N., Singh, S. and Shukla, A. D. 2019. Investigating the sensitivity of glaciers to climate variability since the MIS-2 in the upper Ganga catchment (Saraswati valley), Central Himalaya. *Geomorphology,* **346**, 106854.

Ranhotra, P. S. and Bhattacharyya, A. 2010. Holocene palaeoclimate and glacier fluctuations within Baspa valley, Kinnaur, Himachal Pradesh. *Journal Geological Society of India,* **75:** 527–532.

Ranhotra, P. S., Bhattacharyya, A., Kar, R. and Sekar, B. 2001. Vegetation and climatic changes around Gangotri glacier during Holocene. *Geological Survey of India Special Publication,* **65:** 67–71.

Rao, V. P., Kessarkar, P. M., Patil, S. K. and Ahmad, S. M. 2008. Rock magnetic and geochemical record in a sediment core from the eastern Arabian Sea: Diagenetic and environmental implications during the late Quaternary. *Palaeogeography Palaeoclimatology Palaeoecology,* **270:** 46–52.

Rao, Z., Chen, F., Cheng, H., Liu, W., Wang, G. A., Lai, Z. and Bloemendal, J. 2013. High–resolution summer precipitation variations in the western Chinese Loess Plateau during the last glacial. *Scientific Reports,* **3**: 2785.

Rao, Z., Guo, W., Cao, J., Shi, F., Jiang, H. and Li, C. 2017. Relationship between the stable carbon isotopic composition of modern plants and surface soils and climate: A global review. *Earth Science Reviews,* **165:** 110–119.

Rashid, H., England, E., Thompson, L. and Polyak, L. 2011. Late glacial to Holocene Indian summer monsoon variability based upon sediment. *Terrestrial Atmospheric and Oceanic Sciences,* **22:** 215–228.

Rashid, H., Flower, B. P., Poore, R. Z. and Quinn, T. M. 2007. A 25 ka Indian Ocean monsoon variability record from the Andaman Sea. *Quaternary Science Reviews,* **26:** 2586–2597.

Ratmeyer, V., Balzer, W., Begametti, G., Chiapello, I., Fischer, G., and Wyputta, U. 1999. Seasonal impact of mineral dust on deep-ocean particle flux in the eastern subtropical Atlantic Ocean. *Marine Geology,* **159**: 241–252.

Rawat, S., Gupta, A. K., Sangode, S. J., Srivastava, P. and Nainwal, H. C. 2015. Late Pleistocene–Holocene vegetation and Indian summer monsoon record from the Lahaul, Northwest Himalaya, India. *Quaternary Science Reviews,* **114**: 167–181.

R-Core Team. R. 2017. A Language and Environment for Statistical Computing. R Foundation for Statistical Computing, Vienna, Austria. URL https://www.R–project.org.

Rühland, K., Phadtare, N. R., Pant, R. K., Sangode, S. J. and Smol, J. P. 2006. Accelerated melting of Himalayan snow and ice triggers pronounced changes in a valley peatland from northern India. *Geophysical Research Letters,* **33:** L15709.

Sanwal, J., Kotlia, B. S., Rajendran, C., Ahmad, S. M., Rajendran, K. and Sandiford, M. 2013. Climatic variability in Central Indian Himalaya during the last 1800 years: evidence from a high resolution speleothem record. *Quaternary International,* **304:** 183–192.

Sarkar, A., Mukherjee, A. D., Bera, M. K., Das, B., Juyal, N., Morthekai, P., Deshpande, R. D., Shinde, V. S. and Rao, L. S. 2016. Oxygen isotope in archaeological bioapatites from India: implications to climate change and decline of Bronze Age Harappan civilization. *Scientific Reports,* **6**: 26555. http://dx.doi.org/10.1038/ srep26555.

Sati, S. P., Ali, S. N., Rana, N., Bhattacharya, F., Bhushan, R., Shukla, A. D., Sundriyal, Y. and Juyal, N. 2014. Timing and extent of Holocene glaciations in the monsoon dominated Dunagiri valley (Bangni glacier), Central Himalaya, India. *Asian Earth Science,* **91:** 125–136.

Schulz, H., von Rad, U. and Erlenkeuser, H. 1998. Correlation between Arabian Sea and Greenland climate oscillations of the past 110,000 years. *Nature,* **393:** 54–57.

Sharma, S., Joachimski, M., Sharma, M., Tobschall, H. J., Singh, I. B., Sharma, C., Chauhan, M. S. and Morgenroth, G. 2004. Late glacial and Holocene environmental changes in Ganga plain, Northern India. *Quaternary Science Reviews,* **23:** 145–159.

Shekhar, M., Pal, A. K., Bhattacharyya, A., Ranhotra, P. S. and Roy, I. 2018. Tree–ring based reconstruction of winter drought since 1767 CE from Uttarkashi, Western Himalaya. *Quaternary International,* **479**: 58–69.

Singh, S. K. and Rawat, G. S. 1999. Floral diversity and vegetation structure in great Himalayan National Park, Western Himalaya. *Wildlife Institute of India, Dehradun*.

Sinha, A. K. 1989. Geology of Higher Central Himalayas. John Wiley and Sons, New York, pp. 219.

Sinha, A., Cannariato, K. G., Stott, L. D., Li, H. C., You, C. F., Cheng, H., Edwards, R. L. and Singh, I. B. 2005. Variability of Southwest Indian summer monsoon precipitation during the Bølling–Allerød. *Geology,* **33**: 813–816.

Sirocko, F., Sarnthein, M., Erlenkeuser, H., Lange, H., Arnold, M. and Duplessy, J. C. 1993. Century–scale events in monsoonal climate over

the past 24,000 years. *Nature,* **364:** 322 –324, doi: 10.1038/ 364322a0.

Smol, J. P. 2002. Pollution of Lakes and Rivers—A Paleoenvironmental Perspective. Arnold, London.

Srivastava, P., Agnihotri, R., Sharma, D., Meena, N., Sundriyal, Y. P., Saxena, A., Bhushan, R., Swlani, R., Banerji, U.S., Sharma, C., Bisht, P., Rana, N and Jayangondaperumal, R. 2018. 8000-year monsoonal record from Himalaya revealing reinforcement of tropical and global climate systems since mid-Holocene. *Scientific Reports,* **7**: 14515.

Srivastava, P., Kumar, A., Mishra, A., Meena, N. K., Tripathi, J. K., Sundriyal, Y. P., Agnihotri, R. and Gupta, A. K. 2013. Early Holocene monsoonal fluctuations in the Garhwal higher Himalaya as inferred from multi-proxy data from the Malari paleolake. *Quaternary Research*, **80**(3): 447–458.

Staubwasser, M., Sirocko, F., Grootes, P. M. and Erlenkeuser, H. 2002. South Asian monsoon climate change and radiocarbon in the Arabian Sea during early and middle Holocene. *Paleoceanography and Paleoclimatology*, **17**: 1063.

Stewart, G. R., Turnbull, M. H., Schmidt, S. and Erskine, P. D. 1995. ^{13}C natural abundance in plant communities along a rainfall gradient: a biological integrator of water availability. *Functional Plant Biology,* **22**: 51–55.

Thamban, M., Laluraj, C. M., Naik, S. S. and Chaturvedi, A. 2011. Reconstruction of Antarctic climate change using ice core proxy records from the coastal Dronning Maud Land, East Antarctica. *Journal Geological Society of India,* **78**: 19–29.

Valdiya, K. S. 2001. Reactivation of terrain-defining boundary thrusts in central sector of the Himalaya: implications. *Current Science*, **81**: 1418–1430.

Wang, L., Chen, W., Huang, G. and Zeng, G. 2017. Changes of the transitional climate zone in East Asia: past and future. *Climate Dynamics*, **49:** 1463–1477.

Wang, P., Tian, J., Cheng, X., Liu, C. and Xu, J. 2003. Carbon reservoir changes preceded major ice–sheet expansion at the mid–Brunhes event. *Geology,* **31:** 239–242.

Wang, Y. J., Cheng, H., Edwards, R. L., An, Z. S., Wu, J.Y., Shen, C. C. and Dorale, J. A. 2001. A high–resolution absolute–dated late Pleistocene monsoon record from Hulu Cave, China. *Science,* **294:** 2345–2348.

Wang, Y., Cheng, H., Edwards, R. L., He, Y., Kong, X., An, Z., Wu, J., Kelly, M. J., Dykoski, C. A. and Li, X. 2005. The Holocene Asian monsoon: links to solar changes and North Atlantic climate. *Science,* **308:** 854–857.

Wang, Y., Cheng, H., Edwards, R. L., Kong, X., Shao, X., Chen, S., Wu, J., Jiang, X., Wang, X. and An, Z. 2008. Millennial–and orbital–scale changes in the East Asian monsoon over the past 224,000 years. *Nature,* **451**: 1090.

Webster, P. J., Magana, V. O., Palmer, T. N., Shukla, J., Tomas, R. A., Yanai, M. U. and Yasunari, T. 1998. Monsoons: Processes, predictability, and the prospects for prediction. *Journal Geophysical Research, Oceans,* **103:** 14451–14510.

Witzel, M. 1987. In India and the Ancient world. History, Trade and Culture before A.D. 650. P.H.L. Eggermont Jubilee Volume, (Ed. G. Pollet) Orientalia Lovaniensia Analecta Leuven 253–213.

Witzel, M. 1999. In Aryans and Non–Aryans, Evidence, Interpretation and Ideology (Cambridge: Harvard Oriental Series: Opera Minora **3**: 337–404.

Yadav, R. R. and Singh, J. 2002. Tree–ring–based spring temperature patterns over the past four centuries in western Himalaya. *Quaternary Research,* **57:** 299–305.

Yang, B., Bräuning, A., Dong, Z., Zhang, Z. and Keqing, J. 2008. Late–Holocene monsoonal temperate glacier fluctuations on the Tibetan Plateau. *Global Planetary Change,* **60:** 126–140.

Zheng, S. and Shangguan, Z. 2007. Spatial patterns of foliar stable carbon isotope compositions of C 3 plant species in the Loess Plateau of China. *Ecological Research,* **22:** 342–353.

Manuscript received : April 2019

Manuscript accepted : April 2020